

박 사 학 위 논 문

Doctoral Thesis

통신망에서의 흐름제어에 관한
제어이론적인 접근

A Control-Theoretic Approach to Flow Control in Communication
Networks

조 정 우 (曹 政 佑 Cho, Jeong-woo)

전자전산학과 전기및전자공학전공

Department of Electrical Engineering and Computer Science

(Division of Electrical Engineering)

한 국 과 학 기 술 원

Korea Advanced Institute of Science and Technology

2005

통신망에서의 흐름제어에 관한
제어이론적인 접근

A Control-Theoretic Approach to Flow Control
in Communication Networks

A Control-Theoretic Approach to Flow Control in Communication Networks

Advisor : Professor Song Chong

by

Jeong-woo Cho

Department of Electrical Engineering and Computer Science
(Division of Electrical Engineering)
Korea Advanced Institute of Science and Technology

A thesis submitted to the faculty of the Korea Advanced Institute of Science and Technology in partial fulfillment of the requirements for the degree of Doctor of Philosophy in the Department of Electrical Engineering and Computer Science (Division of Electrical Engineering)

Daejeon, Korea

May 17, 2005

Approved by

Professor Song Chong

Major Advisor

통신망에서의 흐름제어에 관한 제어이론적인 접근

조 정 우

위 논문은 한국과학기술원 박사학위논문으로 학위논문심사
위원회에서 심사 통과하였음.

2005년 5월 17일

심사위원장 정 송 (인)

심사위원 성 단 근 (인)

심사위원 이 황 수 (인)

심사위원 모 정 훈 (인)

심사위원 정 하 응 (인)

DEE 조 정 우. Jeong-woo Cho. A Control-Theoretic Approach to Flow Control in
20025290 Communication Networks. 통신망에서의 흐름 제어에 관한 제어이론적인
 접근. Department of Electrical Engineering and Computer Science (Division
 of Electrical Engineering) . 2005. 77p. Advisor: Prof. Song Chong. Text in
 English.

Abstract

This thesis describes flow control algorithms achieving two kinds of max-min fairness properties, that is to say, *bandwidth max-min* fairness and *utility max-min* fairness and provides a control-theoretic approach to analyze the stability of proposed algorithms. Our algorithms are *scalable* in that routers do not need to store any per-flow information of each flow and they use simple first come first serve (FCFS) discipline, *stable* in that the stability is proven rigorously when there are flows with heterogeneous round-trip delays, and *optimal* in that the gains used for controllers are optimally adjusted.

First, we present a network architecture for the distributed *bandwidth max-min* flow control of elastic flows and generalize stability conditions to enhance network performance. We suggest two closed-loop system models that approximate our flow control algorithms in continuous-time domain where the purpose of the first algorithm is to achieve the target queue length and that of the second is to achieve the target utilization. The slow convergence of many rate-based flow control algorithms, which use queue lengths as input signals, can be resolved by the second algorithm. Based on these models, we find the conditions for controller gains that stabilize closed-loop systems when round-trip delays are equal and extend this result to the case of heterogeneous round-trip delays with the help of Zero exclusion theorem.

Second, we revise the proposed algorithms and provide application-performance oriented flow control algorithms. We present a network architecture for the distributed *utility*

max-min flow control of elastic and non-elastic flows where utility values of users (rather than data rates of users) are enforced to achieve max-min fairness. We also provide a distributed link algorithm that does not use the information of users' utility functions. To show that the proposed algorithm can be stabilized *not locally but globally*, we found that the use of nonlinear control theory is inevitable. The stability of the network is proven by means of so-called loop transformation and absolute stability theorem, viewing the network as a feedback control system with slope-restricted monotone nonlinear feedback. Even though we use a distributed flow control algorithm, it is shown that any kind of utility function can be used as long as the minimum slopes of the functions are greater than a certain positive value. We believe that the proposed distributed algorithm is the first to achieve utility max-min fairness with guaranteed stability in a distributed manner.

We simulate our algorithms with optimal gain sets for various configurations including a multiple bottleneck network to verify the usefulness and extensibility of our algorithms. Our framework lends itself to a single unified flow control scheme that can simultaneously serve, not only elastic flows, but also non-elastic flows such as voice, video and layered video.

Contents

Abstract	i
Contents	iv
List of Figures	viii
List of Tables	x
1 Introduction	1
1.1 Overview and Motivation	1
1.2 Chapter Organization	3
2 Related Works	5
3 Network-Performance Oriented Flow Control	8
3.1 Introduction	8
3.1.1 Our Contributions	9
3.2 Network Model and Controllers	10
3.2.1 PID Link Controller Model	12
3.2.2 PII ² Link Controller Model	13
3.3 Stability Analysis	14
3.3.1 Homogeneous-Delay Case	15

CONTENTS

3.3.2	Explicit Stability Conditions	17
3.3.3	Heterogeneous-Delay Case	19
3.3.4	Stability Analysis for the PII^2 Model	21
3.4	Optimal Controller Gains	22
3.5	Implementation Considerations	26
3.5.1	Determination of Main Parameters	26
3.5.2	Estimation of $ Q_w^l $	27
3.5.3	Discrete-Time Implementations	28
3.6	Simulation Results	28
3.6.1	Scenario 1: Multiple Bottleneck Network With Heterogeneous Round-Trip Delays	29
3.6.2	Scenario 2: Simple Network With Short-lived Flows	32
4	Application-Performance Oriented Flow Control	34
4.1	Introduction	34
4.2	Motivation and Backgrounds for Absolute Stability	37
4.2.1	Motivation	37
4.2.2	Backgrounds for Absolute Stability	38
4.3	Utility Max-Min Architecture	40
4.3.1	PID and PII^2 Link Controller Models	41
4.3.2	Steady State Analysis	42

CONTENTS

4.4	Stability Analysis	43
4.4.1	Homogeneous-Delay Case	44
4.4.2	Graphical Interpretation of Theorem 4.2	46
4.5	Various Utility Functions	48
4.6	Implementation Considerations	51
4.6.1	Estimation of $ Q^l $	51
4.6.2	Discrete-Time Implementations	52
4.6.3	Rate-Based Pricing Scheme	53
4.7	Simulation Results	54
4.7.1	Scenario 1: Simple Network With Heterogeneous Round-Trip Delays	54
4.7.2	Scenario 2: Multiple Bottleneck Network With Heterogeneous Round-Trip Delays	58
5	Conclusion	61
6	Appendix	63
6.1	Proof of Proposition 3.1	63
6.2	Proof of Theorem 3.1	64
6.3	Proof of Corollary 3.1	65
6.4	Proof of Theorem 3.2	66
6.5	Proof of Theorem 4.1	67
6.6	Proof of Theorem 4.2	68

CONTENTS

6.7 Proof of Corollary 4.1	69
6.8 Source Algorithm Revision	71
References	74
Summary (in Korean)	78

List of Figures

3.1	The network architecture for weighted max-min fairness.	11
3.2	Nyquist plot of $G_0(j\omega)$	16
3.3	Explicit stability region in terms of G_D , G_P and G_I	18
3.4	Values of α for $G_D = 0.242$ and $G_D = 0$	24
3.5	Values of α^* for two groups of gain sets.	25
3.6	Multiple bottleneck network used for Scenario 1	29
3.7	Results of Scenario 1: From top to bottom - Queue length at links 1 ($q^1(t)$), Estimated sum of locally bottlenecked flows' weights at link 1 ($ \hat{Q}_w^1 $), Queue length at link 2 ($q^2(t)$), Estimated sum of locally bottlenecked flows' weights at link 2 ($ \hat{Q}_w^2 $) and Source Transmission Rates ($a_i(t)$).	31
3.8	Simple network used for Scenario 2.	33
3.9	Results of Scenario 2: From top to bottom - Queue length at link 3 ($q^3(t)$), Estimated sum of locally bottlenecked flows' weights at link 3 ($ \hat{Q}_w^3 $) and Feedback rate at link 3 ($u^3(t)$).	33
4.1	Bandwidth max-min fairness versus utility max-min fairness.	35
4.2	Two examples of $\phi(\cdot)$ belonging to the sector $[a, b]$	39
4.3	The network architecture for utility max-min fairness.	40
4.4	A block diagram of the proposed architecture.	44
4.5	A block diagram of the proposed architecture after loop transformation.	45
4.6	One sample of $(X(\omega_1), Y(\omega_1))$ plot for G_{PID}^3 with $h = 0.001$	48

LIST OF FIGURES

4.7	Utility functions for different application classes	49
4.8	Simple network used for Scenario 1	55
4.9	Results of Scenario 1 - Queue length at link 1 ($q^1(t)$), Source utilities ($u_i(t)$) and Source sending rates ($a_i(t)$).	56
4.10	Multiple bottleneck network used for Scenario 2	58
4.11	Results of Scenario 2 - Queue length at links ($q^l(t)$), Feedback utilities at links ($u^l(t)$) and Source sending rate of S_1 ($a_1(t)$).	59
4.12	Results of Scenario 2 - Source sending rates of $S_2 \sim S_{14}$ ($a_2(t) \sim a_{14}(t)$).	59
6.1	Nyquist plot used for Proposition 3.1.	64
6.2	Nyquist plot used for Theorem 3.2.	67
6.3	Two samples of $(X(\omega_1), Y(\omega_1))$ plot for G_{PID}^3 and G_{PID}^2	70
6.4	Results of Scenario 1 with the revised source algorithm - Queue length at link 1 ($q^1(t)$), Source utilities ($u_i(t)$) and Source sending rates ($a_i(t)$).	72

List of Tables

3.1	Parameters Used for Simulation.	29
3.2	Flow Models Used for Scenario 1 and Fair Rate. (The units of m_i and Fair rate are in Mbps and the units of D_i are in km. The units of Arrival and Departure time are in seconds.)	30
4.1	Parameters Used for Simulation.	54
4.2	Flow Models Used for Scenario 1.	55
4.3	Flow Models Used for Scenario 2.	58
6.1	Queue Length Overshoots of Scenario 1 for SA and SA'. ($q_T^1 = 68.8\text{kbytes}$)	73

CHAPTER 1

INTRODUCTION

1.1 Overview and Motivation

Recently many efforts have been devoted to provide a framework for designing best-effort service networks that can offer low-loss, low-delay data services where flow control plays a major role in controlling congestion as well as allocating bandwidth among users by enforcing users to adjust their transmission rate in a certain way in response to congestion in their path. The potential advantages of such networks would be the ability to offer even real-time services without the need for complicated admission control, resource reservation or packet scheduling mechanisms.

Flow control is a distributed algorithm to fairly share network bandwidth among competing data sources while maximizing the overall throughput without incurring congestion. The most common understanding of fairness for a best-effort service network is *bandwidth max-min fairness*[†] as defined in [1]. The intuition behind the max-min bandwidth sharing is that any flow is entitled to as much as bandwidth use as is for any other flow with the assumption that all flows have equal priority. This intuition naturally leads to the idea of maximizing the bandwidth use of flows with minimum bandwidth allocation, thus giving rise to the term *max-min flow control*.

The appropriateness of max-min fairness as a bandwidth sharing objective has recently been questioned by Kelly [2] who has introduced the alternative notion of *bandwidth pro-*

[†]To avoid confusion and misunderstandings, note that *max-min fairness* and *bandwidth max-min fairness* are the same property, and *proportional fairness* and *bandwidth proportional fairness* are the same property. We omit the word “bandwidth” for brevity.

portional fairness. The objective of proportional fairness may be interpreted as being to maximize the overall utility of rate allocations assuming each flow has a logarithmic utility function. At first thought, it seems that proportional fairness achieves greater overall throughput than max-min fairness does, by penalizing flows proportional to number of hops in the path in rate allocation [3]. However, this advantage is problematic regarding fairness in that the path of a flow is chosen by the routing protocol in the network, not by the user, so that it is obviously unfair to penalize flows because of their long path length. Furthermore, authors in [4] showed that max-min fairness achieves higher throughput than proportional fairness in some cases. As of now, no one can say that “one is better than the other.” Putting these various facts together, in some cases, one can still argue that max-min fairness might be the better choice than proportional fairness from user’s viewpoint since max-min fairness treats flows equally irrespective of their path length.

Theory and experiments show that as the per-flow product of bandwidth and delay increases, TCP becomes inefficient and prone to instability. In spite of various drawbacks of TCP, it is true that there has been some doubt whether these flow control algorithms will be employed in real networks, e.g., in the Internet. Although most researchers agree that current TCP/IP networks has many defects and only a major and drastic improvement in current networks can overcome such defects, TCP/IP networks are too ubiquitous to be changed. Nevertheless, we take notice of some practical application [5, 6] of these flow control algorithms with keen interest. For example, FAST TCP [5], which originated from various proportional fair flow control algorithms, is considered to be a sincere candidate to replace TCP. Secondly, XCP (eXplicit Control Protocol) [6] is also considered to be a sincere candidate to achieve max-min fairness in the Internet. Although they employ AIMD (additive increase multiplicative decrease) mechanism, note that the mathematical equations describing macroscopic behavior of XCP are the same to those used in [7]. Moreover, authors in [8] showed, through investigating a TCP-RED network with its nonlinear dynamics, that bifurcations occur as various system parameters are varied. These bifurcations, which involve emergence of oscillatory and chaotic behavior, show that nonlinear dynamics ignored in many works [9, 10] should be reconsidered.

The first part of this dissertation concerns the design of *minimum plus weighted max-min flow control* [11], a generalization of bandwidth max-min flow control. In this part, we

review bandwidth max-min flow control algorithms closely and generalize their stability conditions to enhance the performance of communication networks. Through mathematical analysis and computer simulations, we show that our network-performance oriented flow control algorithms greatly outperform previous algorithms while achieving the target queue length of router buffers or the target utilization of links.

Several works including [2, 12–14] imported the concept of *utility* from the science of economics. They are setting a new research trend and replacing traditional research regarding flow control algorithms. Their main contribution is that they opened up an optimization-theoretic approach where each user is associated with a utility function and the network maximizes the aggregate utility. They also introduced the notion of *bandwidth proportional fairness* which is achieved if utility functions are logarithmic. One problem not to be overlooked is that utility functions are restricted to be strictly concave in their works. As pointed out in [15], it is the concavity of utility functions that forces fairness between users in their works. It is emphasized in [16] that some applications apparently have nonconcave utility functions in general. Therefore, there has been eager demand for utility-based flow control algorithms which can support nonconcave utility functions in a distributed manner. In **the second part** of this dissertation, we provide application-oriented flow control algorithms achieving *utility max-min* fairness in a distributed manner. The proposed algorithms enable users to employ arbitrary utility functions as long as the minimum slopes of utility functions are larger than a certain positive value. We resolve several analytical difficulties such as the delays in networks and the nonlinearity of utility functions and find controller gains which stabilize proposed utility max-min networks.

1.2 Chapter Organization

The rest of this dissertation is organized as follows: In Chapter 2, we survey previous works related to flow control in communication networks. In Chapter 3, which corresponds to *the first part*, we provide network-performance oriented flow control algorithms achieving bandwidth max-min fairness and derive stability conditions and optimal controller gains. After considering several implementation issues and presenting several simulation results, we summarize Chapter 3. In Chapter 4, which corresponds to *the second part*, we provide application-performance oriented flow control algorithms achieving utility max-min

fairness. We provide theoretical backgrounds and derive stability conditions which suggest guidelines for deciding shapes of utility functions. After considering several implementation issues and presenting several simulation results, we summarize Chapter 4. In Chapter 5, we conclude this dissertation and suggest some further works. In Chapter 6, several proofs omitted in previous chapters are presented.

CHAPTER 2

RELATED WORKS

Although continual growth of data applications has triggered off the theoretical development of flow control algorithms, there are several major problems that are only partially solved. One of them is round-trip delay caused when feedback congestion signal traverses along its route to deliver itself to the corresponding source. This delay is unpredictable and worse still, can be variational. If all delays of flows are known, we may use optimal control theory [17] in minimizing some performance measure and in globally stabilizing the network. But, this requires that every router knows the variational round-trip delays and that means per-flow information of variational round-trip delays should be stored in every router.

A number of fair rate allocation algorithms [18, 19] have been proposed for ABR service in ATM networks. Since they are performance-oriented heuristic algorithms, they cannot guarantee the asymptotic stability of networks in the presence of round-trip delays. Benmohamed and Meerkov [20] formulated the rate-based flow control problem as a discrete-time feedback control problem with delays. It is notable that they have shown that their proposed algorithm can place the poles of the closed-loop system at arbitrary position in complex plane, yet it still requires that routers know the number of bottlenecked flows for each round-trip delay. In the sequel, we need a scalable and stable flow control algorithm that does not require routers know either per-flow information nor global topology information. Moreover, gain values used for flow control should not be set to conservative values to avoid degradation of overall performance.

Through linearization techniques, many papers such as [9, 10] developed linear dynamic models of TCP to analyze and design Active Queue Management (AQM) control systems.

One advantage of these approaches is that they consider dynamics of TCP which is ubiquitous in current networks. However, as shown in [21], local stability results obtained through linearization techniques cannot guarantee global stability and it is very hard to find *region of attraction* [21] in these works while practical results of their works have motivated many researches. We can see that there are tradeoffs between the rigorousness of analysis and practical value. Moreover, authors in [8] showed, through investigating a TCP-RED network with its nonlinear dynamics, that bifurcations occur as various system parameters are varied. These bifurcations, which involve emergence of oscillatory and chaotic behavior, show that nonlinear dynamics ignored in many works [9, 10] should be reconsidered.

There are some frameworks [12, 13] for controlling flows with heterogeneous round-trip delays based on optimization theory where the optimal solutions are *proportionally fair* in the sense that their aggregate logarithmic utility function is maximized. They require that gains used for their algorithms to depend on the number of flows sharing the most congested link in the network and the longest path used by the sources. Their approaches were focused not on the performance improvement of the transient response but on the establishment of sufficient conditions for stability. Furthermore, to our best knowledge, there has been no optimization-theoretic approaches that guarantees stabilization of queues in routers. It is notable that a paper based on control theory [20] has shown that their proposed algorithm can place the poles of the closed-loop system at arbitrary position in complex plane, yet it still requires that routers know the number of bottlenecked flows for each round-trip delay. In the sequel, we need a scalable and stable flow control algorithm that does not require routers know either per-flow information nor global topology information. Moreover, gain values used for flow control should not be set to conservative values to avoid degradation of overall performance.

In [7], authors proposed a simple proportional integral (PI) flow control algorithm where users' sending rates and the network queues are asymptotically stabilized at a unique equilibrium point at which max-min fairness and target queue lengths of links are achieved. Although the stability of the closed-loop system was analyzed, that was restricted to the case where all round-trip delays are equal. In [22], authors proposed a PID flow control algorithm and found equivalent stability conditions in discrete time domain but did not find an explicit stability region and optimal controller gains.

The rapid growth of multimedia applications has triggered a new fairness concept: *utility max-min fairness*. Originally, Cao and Zegura [16] introduced the concept of utility max-min fairness and motivated application-performance oriented flow control. They emphasized that applications have various kinds of utility function in general. For example, a voice over IP (VoIP) user corresponds to a step-like utility function because his satisfaction is at a maximum if the allowed rate is larger than the voice encoding rate and is at a minimum if the allowed rate is smaller than the encoding rate. The satisfaction of teleconference users with multi-layer streams, consisting of a base-layer stream and multiple enhancement-layer streams, would incrementally increase as additional layers were allowed. Therefore, to accommodate various types of application, it is necessary to relax the restriction on the shapes of utility functions as much as possible. To support various multimedia applications in multirate multicast networks, Rubenstein et al. [23] also employed utility max-min fairness. They showed that if multicast sessions are multirate, the utility max-min fair allocation satisfies desirable fairness properties that do not hold in a single-rate utility max-min fair allocation.

CHAPTER 3

NETWORK-PERFORMANCE ORIENTED FLOW CONTROL

3.1 Introduction

The first part of this dissertation concerns the design of *minimum plus weighted max-min flow control* [11], a generalization of bandwidth max-min flow control, where each flow is associated with two parameters, its weight w_i and minimum rate requirement m_i , such that the minimum rate of each flow is guaranteed as requested during the entire holding time of the flow and the bandwidth unused after allocating the minimum rates is shared by all flows in the weighted max-min sense. An increase in the weight of a flow leads to an increase in the bandwidth share of the flow with the assumption that users pay more for a higher weight. Let us define flow i 's source rate, say a_i , to be $a_i \equiv w_i f_i + m_i$ where f_i is the max-min fair share of the bandwidth unused after allocating the minimum rates to all flows. Let us denote the set of all links, the set of all flows and the set of flows traversing link l by L , N and $N(l)$, respectively. Then, the weighted max-min fairness can be defined as follows.

Definition 3.1: A rate vector $\langle a_1, \dots, a_{|N|} \rangle$ is said to be **feasible** if it satisfies $a_i \geq 0$, $\forall i \in N$ and $\sum_{i \in N(l)} a_i \leq \alpha_T^l \mu^l$, $\forall l \in L$.

Definition 3.2: A rate vector $\langle a_1, \dots, a_{|N|} \rangle$, where $a_i = w_i f_i + m_i$, is said to be **weighted max-min fair** if it is feasible, and for each $i \in N$ and feasible fair rate vector $\langle \bar{f}_1, \dots, \bar{f}_{|N|} \rangle$ for which $f_i < \bar{f}_i$, there exists some i' with $f_i \geq f_{i'} > \bar{f}_{i'}$.

Here μ^l denotes the capacity of link l and α_T^l is a constant defining target link utilization ($0 < \alpha_T^l \leq 1$). Note that admission control is necessary to ensure $\sum_{i \in N(l)} m_i < \alpha_T^l \mu^l$ for all $l \in L$ so that the minimum rate of each flow is guaranteed as requested during the entire holding time of the flow. Definition 3.2 can be restated more informally as follows: a rate vector $\langle a_1, \dots, a_{|N|} \rangle$ is said to be weighted max-min fair if it is feasible and for each user $i \in N$, its fair rate f_i cannot be increased while maintaining feasibility without decreasing the fair rate $f_{i'}$ for some user i' for which $f_{i'} < f_i$.

In this chapter, our goal is to provide a control-theoretic framework based on deterministic fluid models that reveals not only the existence of such a distributed iterative algorithm but also an explicit stability condition of the algorithm in presence of flows with heterogeneous round-trip delays.

3.1.1 Our Contributions

We propose two control-theoretic max-min flow control models and algorithms. The first algorithm satisfies Definition 3.2 for $\alpha_T^l = 1$ such that in the steady-state, bandwidth at every bottleneck link is used to the full while the minimum plus weighted max-min fairness is maintained in bandwidth sharing. Moreover, the queue length at every bottleneck link converges to the target value, say q_T^l , thereby achieving constant queueing delay expressed by $\frac{q_T^l}{\mu^l}$. In contrast, the second algorithm satisfies Definition 3.2 for $0 < \alpha_T^l < 1$ such that in the steady-state, every bottleneck link achieves its target utilization ($\alpha_T^l \mu^l$) and hence virtually zero queueing delay while the minimum plus weighted max-min fairness is maintained. The motivation behind the second algorithm is making the queueing delay at each link to be virtually zero and improving transient performance by absorbing transient overshoots occurring before convergence at the expense of reduced link utilization. But the major advantage of the second algorithm is that the slow adaptation of source rates traversing routers with empty buffers is overcome with this algorithm. The sluggishness of PI controllers based on queue length is also pointed out in [24]. Therefore, the former can offer zero-loss, constant-delay data services at full utilization of bottleneck links whereas the latter can offer zero-loss, zero-delay data services and faster rate adaptation at the expense of reduced bottleneck link utilization.

In the former, the difference between queue length and target queue length, i.e., $q^l(t) - q_T^l$, is used as a congestion measure at each link l and the max-min fair rate f_i is computed

by a PID (proportional integral derivative) controller of this queue-length based congestion measure. In the latter, $\sum_{i \in N(l)} a_i (= w_i f_i + m_i) - \alpha_T^l \mu^l$ is used as a congestion measure at each link l and the max-min fair rate f_i is computed by a PII² (proportional integral double integral) controller of this aggregate-flow based congestion measure. We show that the closed-loop characteristics of the network under these two different algorithms are actually identical, yielding the identical stability condition. By appealing to the Nyquist stability criterion [25] and the Zero exclusion theorem in robust control theory [26], we derive the sufficient and necessary condition for the asymptotic stability of the network as an explicit and usable function of the upper bound $\bar{\tau}$ of all round-trip delays ($\bar{\tau} \geq \tau_i$ for all $i \in N$ where τ_i is the round-trip delay of flow i). Moreover, we find optimal controller gains for both PID and PII² controllers to maximize the asymptotic decay rate of the closed-loop dynamics, thereby achieving faster convergence. Finally, both PID and PII² controllers are highly scalable in that the computational complexity of the link algorithm is $O(1)$ with respect to number of flows passing through a link and no per-flow queueing implementation is necessary at any link.

3.2 Network Model and Controllers

In this section, we propose network models and controllers which achieve weighted max-min fairness. The network architecture with multiple sources and links is depicted in Fig. 3.1. Let us consider a bottleneck link $l \in L$. Then, the dynamics of the buffer of the link can be written by

$$\dot{q}^l(t) = \begin{cases} \sum_{i \in N(l)} a_i(t - \tau_i^{l,f}) - \mu^l, & q^l(t) > 0 \\ \left[\sum_{i \in N(l)} a_i(t - \tau_i^{l,f}) - \mu^l \right]^+, & q^l(t) = 0 \end{cases} \quad (3.1)$$

where $a_i(t)$ is the sending rate of source i , $\tau_i^{l,f}$ is the forward-path delay from source i to link l , μ^l is the link capacity of the link and the saturation function $[\cdot]^+ \equiv \max[\cdot, 0]$ represents that the $q^l(t)$ cannot be negative.

A source i sends packets according to fair rate value assigned by the network. To achieve weighted max-min fairness, let us assume that the source sends packets according to the minimum value among the fair rate values assigned by the links along the path of its flow.

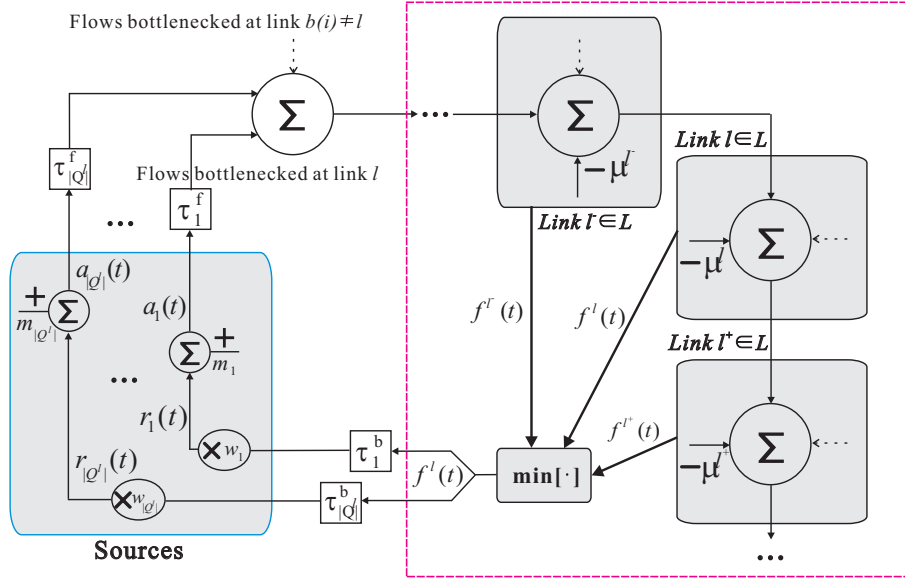


Figure 3.1: The network architecture for weighted max-min fairness.

Thus we assume the following *source algorithm*.

$$\textbf{Source Algorithm: } a_i(t) = m_i + w_i \underbrace{\min_{l \in L(i)} [f^l(t - \tau_i^{l,b})]}_{f_i(t)}, \quad (3.2)$$

where $L(i)$ is the set of links which flow i traverses, $f^l(t)$ is the rate value assigned by the link l on the path of flow i and $\tau_i^{l,b}$ is the backward-path delay from link l to source i . Because $\min[\cdot]$ operation is taken over a finite number of links, there should exist at least one link l such that $f^l = \min[\cdot]$. Therefore, each flow i has at least one bottleneck $l \in L(i)$. There are several assumptions employed for the analysis of the network model.

- A.1. We assume that the sources are *persistent* until the closed-loop system reaches steady state. By ‘persistent’, we mean that the source always has enough data to transmit at the allocated rate.
- A.2. We assume that the available link capacity μ^l is constant until the system reaches steady state. Also, the buffer size at this link is assumed infinite.

A.3. There are two delays, say, the forward-path delay $\tau_i^{l,f}$ and the backward-path delay $\tau_i^{l,b}$, which include propagation, queueing, transmission and processing delays. We denote the sum of two delays by τ_i and assume that this is constant.

3.2.1 PID Link Controller Model

To control flows and to achieve weighted max-min fairness, we use a PID link controller at each link. In the PID link controller model, there is a specified target queue length q_T^l to avoid underutilization of the link capacity. Because we have a nonzero target queue length q_T^l , the PID model implies that $\alpha_T^l = 1$ in Definition 3.1. Each link calculates the common feedback rate value $f^l(t)$ for all flows traversing the link according to the PID control mechanism.

In general, a proportional term increases the convergence speed of transient responses and reduces errors caused by disturbances. An integral term can effectively eliminate steady state error and results in the size of the stability region being reduced. A derivative term adds some damping and extends the area of the stability region. It also improves the performance of the transient period.

Let us denote the set of flows bottlenecked at link l and its cardinality by Q^l and $|Q^l|$. The link algorithm with the PID controller that uses the difference between $q^l(t)$ and q_T^l as its input is given by

$$\textbf{Link Algorithm 1: } f^l(t) = \left[-\frac{1}{|Q_w^l|} \left(g_P e_1^l(t) + g_I \int_0^t e_1^l(t) dt + g_D \dot{e}_1^l(t) \right) \right]^+ \quad (3.3)$$

where $e_1^l(t) \equiv q^l(t) - q_T^l$ is the error signal between control target and current output signal and, $g_P > 0$ and $g_I, g_D \geq 0$. Here, $|Q_w^l|$ denotes the sum of locally bottlenecked flows' weights, i.e., $|Q_w^l| \equiv \sum_{i \in Q^l} w_i$. For convenience in deriving our results, we use the definition $\rho_i \equiv w_i / |Q_w^l|$. Then it is satisfied that $\sum_{i \in Q^l} \rho_i = 1$ and $\rho_i > 0$ because we require $w_i > 0$.

Suppose that the closed-loop system has an equilibrium point at which the derivatives of the system variables are zero, i.e., $\lim_{t \rightarrow \infty} \dot{q}^l(t) = 0$, $\lim_{t \rightarrow \infty} q^l(t) = q_T^l$, $\lim_{t \rightarrow \infty} a_i(t) = a_{is}$ and $\lim_{t \rightarrow \infty} f^l(t) = f_s^l$. To be more formal, the set of flows bottlenecked at link l is given by

$$Q^l = \{i | i \in N(l) \text{ and } a_{is} = w_i f_s^l + m_i\} \quad (3.4)$$

and the set of all flows not bottlenecked at link l but traversing link l , $N(l) - Q^l$, is given by

$$N(l) - Q^l = \{i | i \in N(l) \text{ and } a_{is} = w_i f_s^{b(i)} + m_i \text{ and } f_s^{b(i)} < f_s^l\} \quad (3.5)$$

where $b(i) \in L(i)$ ($b_i \neq l$) is some bottleneck for flow $i \in N(l) - Q^l$. If we assume that $Q^l \neq \emptyset$, the equation (3.1) implies that the link capacity μ^l in the PID link controller model is fully utilized as follows.

$$\sum_{i \in N(l)} a_{is} = \mu^l. \quad (3.6)$$

Using (3.6), and the definitions (3.4) and (3.5), we obtain

$$\sum_{i \in Q^l} (w_i f_s^l + m_i) + \sum_{i \in N(l) - Q^l} (w_i f_s^{b(i)} + m_i) = \mu^l$$

which establishes that the PID link controller model achieves the following *weighted max-min fairness property*

$$r_{is} \equiv w_i f_s^l = \frac{w_i}{|Q_w^l|} \left(\mu^l - \sum_{i \in N(l) - Q^l} w_i f_s^{b(i)} - \sum_{i \in N(l)} m_i \right). \quad (3.7)$$

3.2.2 PII² Link Controller Model

Instead of using $e_1^l(t)$, one can use $e_2^l(t) \equiv \sum_{i \in N(l)} a_i(t - \tau_i^{l,f}) - \alpha_T^l \mu^l$ as an input of link controllers where α_T^l is the target utilization of link l and should be a positive value smaller than 1. In this case, one can use a PII² link controller model as follows because we now use rate error signal instead of queue error signal.

Link Algorithm 2:
$$f^l(t) = \left[-\frac{1}{|Q_w^l|} \left(h_P e_2^l(t) + h_I \int_0^t e_2^l(t) dt + h_{I^2} \int_0^t \int_0^t e_2^l(t) dt dt \right) \right]^+ \quad (3.8)$$

where $h_P, h_{I^2} \geq 0$ and $h_I > 0$. It should be remarked that the PID and PII² model are not identical because $\dot{e}_1^l(t) = \dot{q}^l(t) = \sum_{i \in N(l)} a_i(t - \tau_i^{l,f}) - \mu^l \neq e_2^l(t)$ for $q^l(t) > 0$. In this model, the purpose of control is to achieve the target utilization, α_T^l . In the PII² model, note that $\dot{q}^l(t) = -(1 - \alpha_T^l) \mu^l < 0$ when $q^l(t) > 0$ and $e_2^l(t) = 0$. Therefore, this model controls flows so that the queue length at steady state becomes zero at the cost of some degree of underutilization. In the PID model, note that $e_1^l(t)$ cannot be smaller than

$-q_T^l$ because $q^l(t)$ cannot be negative. Thus, one axiomatic advantage of the PII^2 model is that the control dynamics are not saturated at $q^l(t) = 0$ because the controller uses the rate error signal as its input instead of the queue error signal. Thus the main physical saturation nonlinearity of the PID model can be overcome by this model.

For steady state analysis, following a similar way given in Section 3.2.1 except that $\mu^l \rightarrow \alpha_T^l \mu^l$ and $\lim_{t \rightarrow \infty} q^l(t) = 0$, r_{is} is given as follow.

$$r_{is} \equiv w_i f_s^l = \frac{w_i}{|Q_w^l|} \left(\alpha_T^l \mu^l - \sum_{i \in N(l) - Q^l} w_i f_s^{b(i)} - \sum_{i \in N(l)} m_i \right). \quad (3.9)$$

This shows that the PII^2 model also achieves *weighted max-min fairness property*.

3.3 Stability Analysis

Although we presented a multiple bottleneck network architecture in Section 3.2, rigorous stability analysis of these kinds of models has been shown to be very difficult in [27] due to the dynamics coupling among links that operate on a “first come first serve” (FCFS) principle. In [27], though such dynamics coupling exists in theory, the effect of coupling was shown to be negligible through simulations. Recently, Wydrowski et al. [28] also showed that the dynamics coupling is of a very weak form. Thus, in this section, *we drop the superscript l and the analysis is focused on a single bottleneck model*. We conjecture that our analytical results can be extended to multiple bottleneck models without significant modification.

We describe the stability conditions for controller gains for two network models when the saturation functions employed in Eqs. (3.1), (3.3) and (3.8) are relaxed. The main contribution of our analysis is that we find the *equivalent* stability condition in continuous-time domain for the case flows experience heterogeneous round-trip delays, and the stability condition depends only on a given upper bound of round-trip delays. At first, we concentrate on the PID link controller model and similar arguments for the PII^2 link controller model will be given in Section 3.3.4.

3.3.1 Homogeneous-Delay Case

To analyze the homogeneous-delay case of the PID model, we simply set $|Q|$ to be 1, then there is only one flow which is bottlenecked at the link. We also regard this case as the situation where all round-trip delays of flows are equal and ρ_i are chosen to be $\rho_i = w_i/|Q_w|$, $\forall i \in Q$. This case allows us to drop the subscript of τ_1 , so that the round-trip delay of flow 1 be τ . By the homogeneous-delay assumption, ρ_i can be set as follows.

$$\rho_1 = \frac{w_1}{|Q_w|} = 1 \quad \text{and} \quad \rho_i = 0, \quad \forall i > 1. \quad (3.10)$$

By Eq. (3.3) and plugging Eq. (3.2) into Eq. (3.1), we can get the following equations.

$$\begin{aligned} \ddot{e}_1(t) &= w_1 \dot{f}(t - \tau), \\ \dot{f}(t) &= -\frac{1}{|Q_w|} [g_P \dot{e}_1(t) + g_I e_1(t) + g_D \ddot{e}_1(t)]. \end{aligned}$$

Then the Laplace transform of the open-loop system is given by

$$G(s) \equiv \underbrace{\left(g_D + \frac{g_P}{s} + \frac{g_I}{s^2} \right)}_{G_0(s)} \exp(-\tau s) \quad (3.11)$$

which corresponds to the open-loop transfer function of the PID model. By $s = j\omega$, the following equations, to which we now apply Nyquist stability criterion [25], are obtained.

$$G(j\omega) = G_0(j\omega) \exp(-j\tau\omega), \quad G_0(j\omega) = g_D - j\frac{g_P}{\omega} - \frac{g_I}{\omega^2}. \quad (3.12)$$

Note that the Nyquist plot of $G_0(j\omega)$, which is depicted in Fig. 3.2 starts in the third quadrant and ends at g_D where $\omega = +\infty$. Inferring from Fig. 3.2, we can see that the condition $|g_D| < 1$ is necessary because the Nyquist plot of $G(j\omega)$ will encircle or touch $-1 + j0$ unless the condition is satisfied.

Let us denote by P and $\bar{\omega}$ the point at which Nyquist plot of $G_0(j\omega)$ intersects with the unit circle and the value of ω at P , respectively. As shown in Fig. 3.2, ϕ is the angle between P and $-1 + j0$. More precisely,

$$\phi = \arccos(-\text{Re}[G_0(j\bar{\omega})]). \quad (3.13)$$

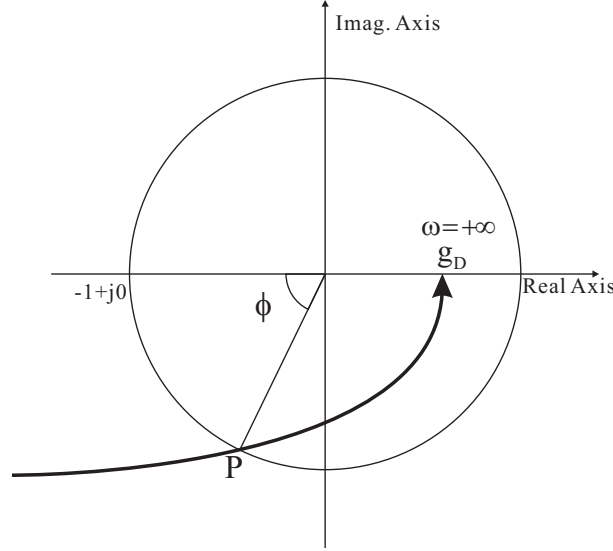


Figure 3.2: Nyquist plot of $G_0(j\omega)$.

Since the Nyquist plot of $G(j\omega)$ is the Nyquist plot of $G_0(j\omega)$ rotated by $\tau\omega$ in the clockwise direction, it is required by Nyquist stability criterion that $\tau\omega < \phi$. Before proving the theorem for homogeneous-delay case, we need the following proposition. (Its proof is in Appendix 6.1.)

Proposition 3.1: If there exists a unique value $\bar{\omega} \in (0, \pi/\tau)$ such that $|G(j\bar{\omega})| = 1$, $\text{Im}[G(j\bar{\omega})] < 0$, and $|G(j\omega)| > 1$ for all $\omega < \bar{\omega}$, then $\text{Im}[G(j\omega)] < 0$ is satisfied for all ω in $0 < \omega \leq \bar{\omega}$.

With the help of Proposition 3.1, the equivalent stability condition for the homogeneous-delay case now can be stated as follows. (Its proof is in Appendix 6.2.)

Theorem 3.1 (Homogeneous-Delay Case, PID Model): The closed-loop system of the PID model with a homogeneous delay $\tau \geq 0$ is asymptotically stable if and only if $|g_D| < 1$ and the delay is bounded by

$$0 \leq \tau < \frac{\arccos\left(\frac{g_L}{\bar{\omega}^2} - g_D\right)}{\bar{\omega}}. \quad (3.14)$$

3.3.2 Explicit Stability Conditions

Although we acquired the equivalent condition for the stability of our closed-loop system, the conditions are implicit and do not allow easy choice of controller gains, g_P , g_I and g_D . To obtain more explicit stability conditions, we proceed in the following way.

We assume that τ is fixed to a value and that $g_D \geq 0$, $g_P > 0$ and $g_I \geq 0$. We will find explicit conditions for controller gains. Now, there are three variables, i.e., g_P , g_I and g_D , concerned with the stability conditions. For mathematical tractability, we will ignore the case $\tau = 0$ and use the following definitions of variables.

$$\omega_1 \equiv \bar{\omega}\tau, \quad G_D \equiv g_D, \quad G_P \equiv g_P\tau, \quad G_I \equiv g_I\tau^2.$$

If we rewrite Eq. (3.14) and the condition for $\bar{\omega}$ in terms of new variables assuming $\tau > 0$, it follows that

$$0 < \omega_1 < \arccos\left(\frac{G_I}{\omega_1^2} - G_D\right) \quad (3.15)$$

$$\text{and} \quad \left(\frac{G_I}{\omega_1^2} - G_D\right)^2 + \left(\frac{G_P}{\omega_1}\right)^2 = 1. \quad (3.16)$$

Corollary 3.1 (Explicit Stability Region): The stability condition given in Theorem 3.1 is equivalent to the following equations.

$$0 \leq G_D < 1, \quad (3.17)$$

$$0 < G_P < \begin{cases} \arccos(-G_D)\sqrt{1-G_D^2} & \text{if } 0 \leq G_D < -\cos(\omega_0), \\ \omega_0 \sin(\omega_0) & \text{if } -\cos(\omega_0) \leq G_D < 1, \end{cases} \quad (3.18)$$

$$\begin{cases} 0 \leq G_I < \omega_{*1}^2(G_D + \cos(\omega_{*1})) & \text{if } \arccos(-G_D) \leq \omega_0, \\ \omega_{*2}^2(G_D + \cos(\omega_{*2})) < G_I < \omega_{*1}^2(G_D + \cos(\omega_{*1})) & \text{if } \omega_0 < \arccos(-G_D), \end{cases} \quad (3.19)$$

where $\omega_0 \approx 2.03$ is the value maximizing the function $\omega \sin(\omega)$ over the interval $0 < \omega < \pi$, ω_{*1} is the unique solution of $G_P = \omega \sin(\omega)$ over the interval $0 < \omega \leq \omega_0$, and ω_{*2} is the unique solution of $G_P = \omega \sin(\omega)$ over the interval and $\omega_0 < \omega < \arccos(-G_D)$ which exists only when the condition $\omega_0 < \arccos(-G_D)$ is satisfied.

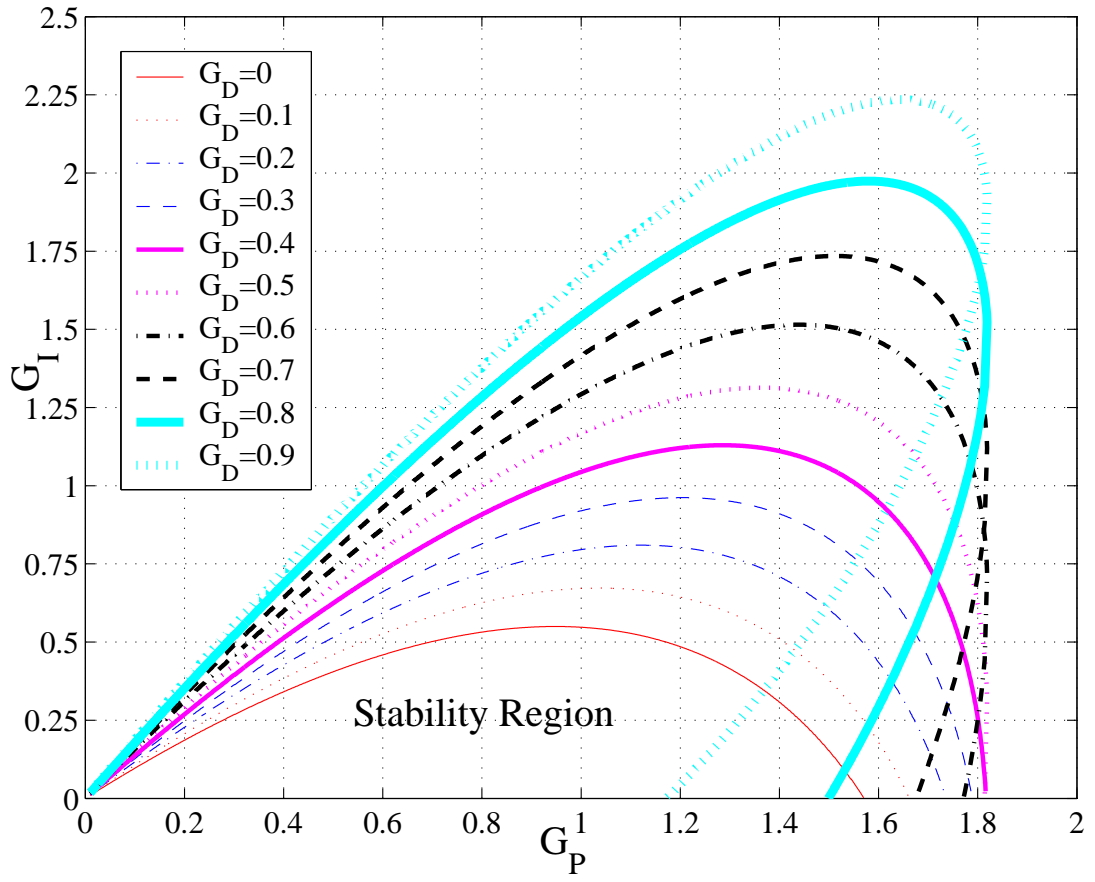


Figure 3.3: Explicit stability region in terms of G_D , G_P and G_I .

Remark 3.1 (Essential Controller Term): From Corollary 3.1, we can see that G_D can be 0. Then the stability condition for controller gains becomes as follows:

$$0 < G_P < \frac{\pi}{2},$$

$$0 \leq G_I < \omega_{*1}^2 \cos(\omega_{*1}).$$

Similarly, the stability condition when $G_D = G_I = 0$ is $0 < G_P < \pi/2$. One can verify that the essential controller term that should be positive is P-term and the other two terms are used for performance improvement. In fact, when $G_D = G_I = 0$ and $G_P > 0$, the performance of closed-loop systems is very poor. Since the essential controller term is P-term, one can consider any combinations including P-term such as P, PI, PII², PII²I³, PID, PIDD², etc. The main reason for choosing the PID model lies in its simplicity and efficiency. For example, if we consider the PIDD² model, we have to estimate the second derivative term of the queue length $e_1^l(t) = q^l(t) - q_T^l$ and the analysis of the PIDD² model is much harder than that of the PID model. Similarly, the essential controller term for PII² model is I-term.

The proof of this corollary is in Appendix 6.3. This corollary allows us to draw an exact stability region, provided that we are given a value of G_D . With the help of Corollary 3.1, an explicit stability region is depicted in Fig. 3.3 for various values of G_D . Notably, stability region corresponding to $G_D = 0$ is exactly the same to the stability region found in [7] where PI controller was used for flow control.

3.3.3 Heterogeneous-Delay Case

In this section, we prove a theorem that allows us to control flows with heterogeneous round-trip delays only with the knowledge of a given upper bound of round-trip delays. This point is important because a router may not store round-trip delay values of flows because doing so inevitably compels a router to store per-flow information.

With cancellation of Eq. (3.10), we now consider more general situation where all round-trip delays of flows can be different and the sum of ρ_i is less than or equal to 1. The reason for allowing $\sum_{i \in Q} \rho_i < 1$ will be clear soon. Similar to Section 3.3.1, we can get the following open-loop transfer function.

$$G(s) \equiv \underbrace{\left(g_D + \frac{g_P}{s} + \frac{g_I}{s^2} \right)}_{G_0(s)} \sum_{i \in Q} \rho_i \exp(-\tau_i s). \quad (3.20)$$

Before proving the theorem, we need a proposition.

Proposition 3.2 (-1+j0 Exclusion Theorem): Given a fixed value ω , let us define the value set

$$V(\omega) = \left\{ Z = G(j\omega, \boldsymbol{\rho}, \boldsymbol{\tau}) \mid \sum_{i \in Q} \rho_i \leq 1, 0 \leq \tau_i \leq \tau \right\}$$

where $\boldsymbol{\rho} = (\rho_1, \dots, \rho_{|Q|})$ and $\boldsymbol{\tau} = (\tau_1, \dots, \tau_{|Q|})$. The system is asymptotically stable if and only if the following two conditions are satisfied:

- There exists a $2|Q|$ -tuple vector $(\rho_1, \dots, \rho_{|Q|}, \tau_1, \dots, \tau_{|Q|})$ such that the system with the open-loop transfer function of $G(s, \boldsymbol{\rho}, \boldsymbol{\tau})$ is asymptotically stable.
- For all $\omega \geq 0$, the value set $V(\omega)$ does not touch the point $-1 + j0$, i.e., $-1 + j0 \notin V(\omega)$.

Basically, this proposition is a direct application of the *Zero exclusion theorem* which is one of main results in robust control theory. Explanation and proof of the theorem can be found in [26, 29]. Denoting by $\bar{\tau}$ an upper bound of τ_i , i.e., $\max_{i \in Q} \tau_i \leq \bar{\tau}$, we are ready to state our main result. (Its proof is in Appendix 6.4.)

Theorem 3.2 (Heterogeneous-Delay Case, PID Model): The closed-loop system of the PID model with heterogeneous delays is asymptotically stable for all $0 \leq \tau_i \leq \bar{\tau}$ and for all ρ_i satisfying $\sum_{i \in Q} \rho_i \leq 1$ if and only if the closed-loop system of the homogeneous-delay case with delay $\bar{\tau}$ is asymptotically stable.

This theorem guarantees that a network is stabilized for all combinations of $0 \leq \tau_i \leq \bar{\tau}$ if routers know only one upper bound of round-trip delays, i.e., $\bar{\tau}$, by choosing a controller gain set $(G_D, G_P, G_I) = (g_D, g_P \bar{\tau}, g_I \bar{\tau}^2)$ contained in stability region depicted in Fig. 3.3. Observe that the closed-loop dynamics should be better when the $\bar{\tau}$ is more tightly chosen. A method for the estimation of $|Q_w|$ will be explored in Section 3.5.2 because a router without per-flow information cannot know the exact sum of w_i . By appealing to Theorem 3.2, we can see that it is *completely safe* to overestimate $|Q_w|$, i.e., $|\hat{Q}_w| \geq |Q_w|$ where $|\hat{Q}_w|$ is the estimate of $|Q_w|$, because $\sum_{i \in Q} \rho_i = \sum_{i \in Q} w_i / |Q_w|$ is allowed to be smaller than 1.

3.3.4 Stability Analysis for the PII² Model

In this section, we show that the stability arguments given so far can be applied to the PII² model without any modification. For the PII² model, by plugging Eq. (3.2) into Eq. (3.1) and using the relation $\dot{e}_2(t) = \ddot{e}_1(t)$, we can get the following equation.

$$\ddot{e}_2(t) = \ddot{e}_1(t) = \sum_{i \in Q} w_i \ddot{f}(t - \tau_i), \quad (3.21)$$

From Eq. (3.8), we can get the following equation.

$$\ddot{f}(t) = -\frac{1}{|Q_w|} [h_P \ddot{e}_2(t) + h_I \dot{e}_2(t) + h_{I^2} e_2(t)]. \quad (3.22)$$

Thus the open-loop transfer function becomes

$$G(s) \equiv \underbrace{\left(h_P + \frac{h_I}{s} + \frac{h_{I^2}}{s^2} \right)}_{G_0(s)} \sum_{i \in Q} \rho_i \exp(-\tau_i s). \quad (3.23)$$

By comparing Eq. (3.20) and (3.23) carefully, one can observe that the two equations are the same if the following substitutions are used.

$$h_P = g_D, \quad h_I = g_P, \quad h_{I^2} = g_I. \quad (3.24)$$

Because the Nyquist stability criterion and Zero exclusion theorem are related only to the open-loop transfer functions, we can now state the following theorem.

Theorem 3.3 (Homogeneous/Heterogeneous-Delay, PII² Model): By using the Eq. (3.24), the stability conditions of the PII² model for the homogeneous-delay and heterogeneous-delay case are respectively given by Theorem 3.1 and 3.2.

Thus the stability of the PII² model can be determined by checking the residence of the gains $G_D = H_P$, $G_P = H_I$ and $G_I = H_{I^2}$ in the stability region given in Fig. 3.3 by defining the gains H_P , H_I and H_{I^2} as follows.

$$H_P \equiv h_P, \quad H_I \equiv h_I \bar{\tau}, \quad H_{I^2} \equiv h_{I^2} \bar{\tau}^2.$$

3.4 Optimal Controller Gains

Although we found the equivalent conditions for stability, choosing controller gains is still an open problem, because there is no well-established method for choosing gains. In this section, we provide one approach for choosing controller gains where the asymptotic decay rates of closed-loop system are maximized.

At first we focus on the PID model. From Eqs. (3.1), (3.2) and (3.3), we can get the following closed-loop equation.

$$\ddot{e}_1(t) + \sum_{i \in Q} \rho_i [g_D \ddot{e}_1(t - \tau_i) + g_P \dot{e}_1(t - \tau_i) + g_I e_1(t - \tau_i)] = 0, \quad (3.25)$$

For the PII^2 model, we also get the same closed-loop equation from Eqs. (3.21) and (3.22) with change of variables, i.e., $e_1(t) \rightarrow e_2(t)$, $g_D \rightarrow h_P$, $g_P \rightarrow h_I$ and $g_I \rightarrow h_{I^2}$. Because all arguments in this section will depend only on the closed-loop equation, we can see they can be applied to the PII^2 model identically.

Generally, Eq. (3.25) has infinite number of eigenvalues. Because a router without per-flow information cannot know per-flow round-trip delays τ_i , for the time being, we assume that $\tau_i = \bar{\tau}$, $\forall i \in Q$. Then, with change of variables, $t = \bar{\tau}\eta$, Eq. (3.25) becomes

$$\ddot{e}_1(\eta) + G_D \ddot{e}_1(\eta - 1) + G_P \dot{e}_1(\eta - 1) + G_I e_1(\eta - 1) = 0 \quad (3.26)$$

where $G_D = g_D$, $G_P = g_P \bar{\tau}$ and $G_I = g_I \bar{\tau}^2$. Then its characteristic equation becomes

$$H(z) \equiv z^2 e^z + G_D z^2 + G_P z + G_I = 0. \quad (3.27)$$

Any solution to the Eq. (3.26) can be represented by the following series expansion [30,31],

$$e_1(\eta) = \sum_{n=1}^{\infty} p_n(\eta) \exp(z_n \eta) \quad (3.28)$$

where $p_n(\eta)$ is a suitable polynomial and z_n are the roots of the corresponding characteristic equation (3.27). Let us consider the principal root, denoted by z^* , which is the root having the largest real part. By letting $z^* = -\alpha + j\beta$, where $\alpha > 0$ and $\beta \in \mathcal{R}$, it follows from (3.28) that

$$e_1(\eta) \approx c_1 \exp(z^* \eta), \quad (3.29)$$

$$\|e_1(\eta)\| \leq c_2 \exp(-\alpha\eta) \text{ for large } \eta,$$

where c_1 and c_2 are constants and $\|\cdot\|$ denotes the Euclidean norm. In terms of the original variable $t(= \bar{\tau}\eta)$, it becomes

$$\|e_1(t)\| \leq c_2 \exp(-\frac{\alpha}{\bar{\tau}}t) \text{ for large } t. \quad (3.30)$$

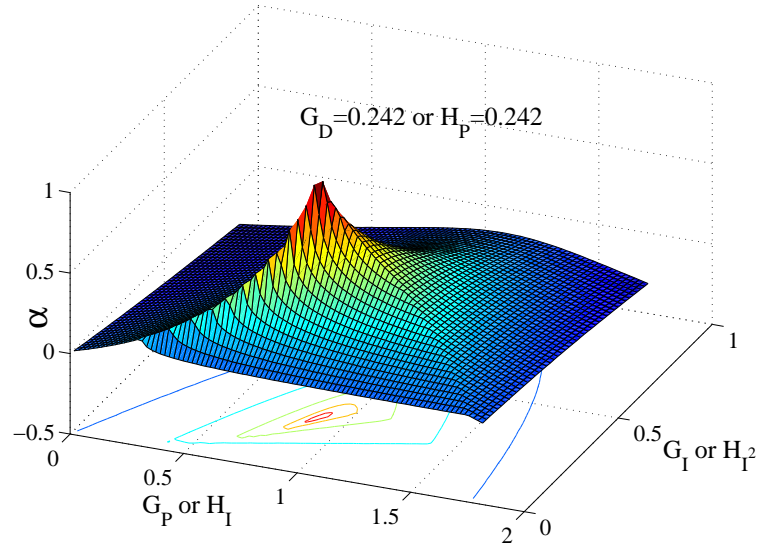
Note that $\alpha/\bar{\tau}$ is the asymptotic decay at which the closed-loop system tends to the equilibrium point. We could find controller gain sets maximizing the value of α by extensive numerical calculations with the help of graphical analysis. Because the derivative term in PID control model and the proportional term in PII² control model are not necessarily required, we can also use two-term controllers, i.e., PI controller or II² controller, to allow simpler implementation. The PID, PI, PII² and II² controller gain sets which maximize the values of α are respectively given as

$$\begin{aligned} G_{PID}^3 &\equiv (G_D, G_P, G_I) = (0.242, 0.868, 0.261), \\ G_{PID}^2 &\equiv (G_D, G_P, G_I) = (0, 0.482, 0.091), \\ G_{PII^2}^3 &\equiv (H_P, H_I, H_{I^2}) = G_{PID}^3, \\ G_{PII^2}^2 &\equiv (H_P, H_I, H_{I^2}) = G_{PID}^2 \end{aligned}$$

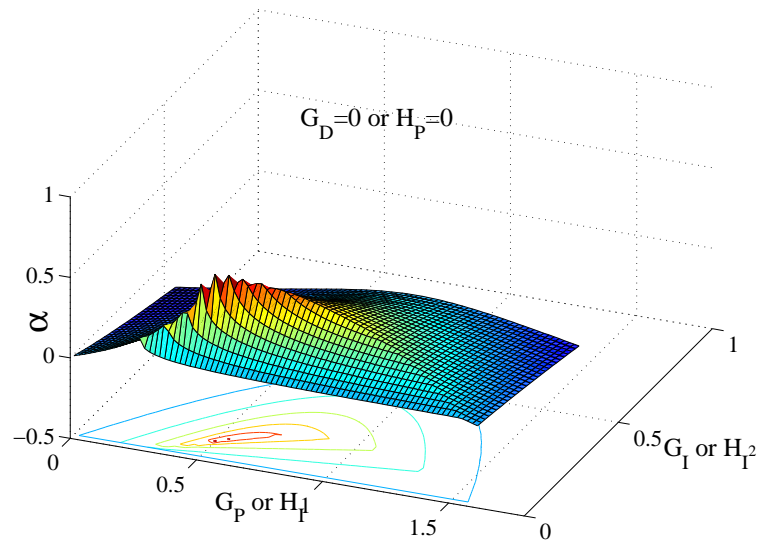
where G_{PID}^3 and G_{PID}^2 are for the PID model and $G_{PII^2}^3$ and $G_{PII^2}^2$ are for the PII² model. For two groups of gain sets, the values of α are 1.16 and 0.56 respectively. Inferring from the values of α , we can expect that a system with a three-term controller (PID or PII²) converges approximately twice faster than that with a two-term controller (PI or II²) does. For two cases, i.e., $G_D = 0.242$ and $G_D = 0$, values of α are depicted in Fig. 3.4.

Because we assumed that $\tau_i = \bar{\tau}$, $\forall i \in Q$, it is not clear what the asymptotic decay rate would be if there exist flows with $\tau_i < \bar{\tau}$. Let us consider flows traversing the link of interest with round-trip delay to be $\tau_i = \tau < \bar{\tau}$. For a given gain set (G_D, G_P, G_I) , if the link uses $\bar{\tau}$ in calculation of (g_D, g_P, g_I) , then the link will control the flow with gains $(g_D, g_P, g_I) = (G_D, G_P/\bar{\tau}, G_I/\bar{\tau}^2)$ and the corresponding asymptotic decay rate will be α/τ where α is obtained with the following actual gain set.

$$(G_D^*, G_P^*, G_I^*) = (G_D, G_P\tau/\bar{\tau}, G_I\tau^2/\bar{\tau}^2).$$

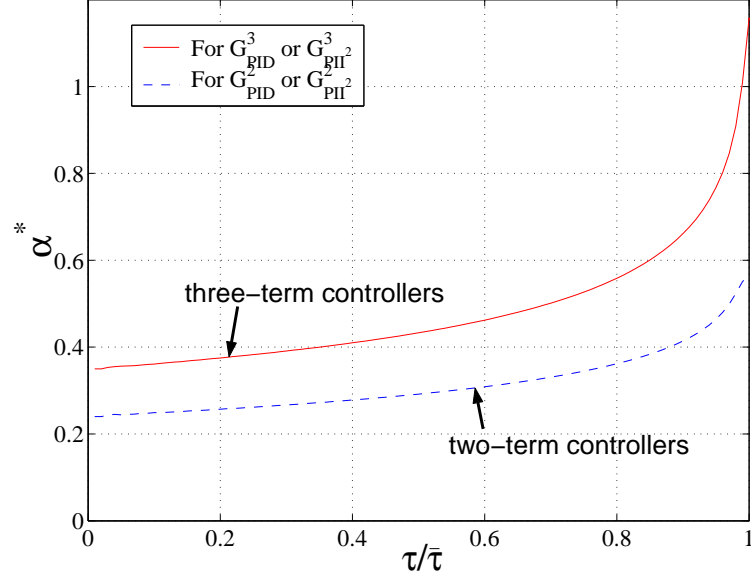


(a) For $G_D = 0.242$



(b) For $G_D = 0$

Figure 3.4: Values of α for $G_D = 0.242$ and $G_D = 0$.


 Figure 3.5: Values of α^* for two groups of gain sets.

To fairly compare the asymptotic decay rates, we can rewrite α/τ and Eq. (3.30) as follows

$$||e_1(t)|| \leq c_3 \exp(-\frac{\alpha^*}{\bar{\tau}}t) \text{ for large } t, \alpha^* \equiv \alpha \frac{\bar{\tau}}{\tau}.$$

For two groups of gain sets, values of α^* versus $\tau/\bar{\tau}$ are depicted in Fig. 3.5. It is seen that asymptotic decay rates of three-term controller gain sets (G_{PID}^3 and G_{PII2}^3) are at least 1.45 times larger than those of two-term controller gain sets (G_{PID}^2 and G_{PII2}^2). As $\tau/\bar{\tau}$ approaches unity, the gaps of asymptotic decay rates between two gain sets increases. As $\tau/\bar{\tau}$ approaches zero, asymptotic decay rates of two cases converge to 0.35 and 0.24 respectively. In fact, one can get following result from the Laplace transform of Eq. (3.25) assuming that $\tau_i = \tau$, $\forall i \in Q$ and $(g_D, g_P, g_I) = (G_D, G_P/\bar{\tau}, G_I/\bar{\tau}^2)$.

$$\lim_{\tau \rightarrow 0} \alpha^* = \text{Re} \left[\frac{G_P - \sqrt{G_P^2 - 4G_I(1 + G_D)}}{1 + G_D} \right]$$

In the sequel, we can conjecture that for all combinations of $\tau_i \leq \bar{\tau}$, $\forall i \in Q$, the value of α^* given in Eq. (3.30) will be in the interval $[0.35, 1.16]$ when three-term controllers are used and in the interval $[0.24, 0.57]$ when two-term controllers are used.

3.5 Implementation Considerations

3.5.1 Determination of Main Parameters

Here we provide methods for determining main parameters of two models. In the PID model, $\bar{\tau}^l$, the upper bound of round-trip delays among all paths traversing the link l , and q_T^l , the target queue length at link l are closely related to each other. Let p_l be the set of all round-trip paths traversing link l . Let us consider a sample round-trip path $p \in p_l$ traversing the link l , i.e., $p = \langle l_1, \dots, l_{|L_p|} \rangle$, $l_i \in L$ where $L_p = \{l_1, \dots, l_{|L_p|}\}$ and $|L_p|$ is the cardinality of L_p . At the worst, there may exist locally bottlenecked flows for any link $l_i \in L_p$. Let us assume that the sum of flows' weights is sufficiently large, i.e., $|Q_w^l| \gg 1$, such that the target queue lengths of all links are achieved even in transient state. Then, $\bar{\tau}^l$ should satisfy the following equation.

$$\bar{\tau}^l \geq \tau_{prop_p} + \sum_{l \in L_p} \frac{q_T^l}{\mu^l}, \quad \forall p \in p_l \quad (3.31)$$

where τ_{prop_p} is the round-trip propagation delay on the path p and μ^l is the available link capacity of link l . Let us consider a near-worst case situation where two flows are bottlenecked at the link $l \in L_p$, and suddenly flow 1 which has sent data at a rate close to μ_l stops its transmission abruptly. Thus, q_T^l , the target queue length of link l , should be set to $\beta \bar{\tau}^l \mu^l$ where β is a constant, because the worst-case queue length undershoot is proportional to $\bar{\tau}^l \mu^l$. Thus, Eq. (3.31) becomes

$$\bar{\tau}^l \geq \frac{\tau_{prop_p}}{1 - |L_p|\beta} \quad \text{and} \quad 1 - |L_p|\beta > 0, \quad \forall p \in p_l > 0.$$

We can see that $\beta < 1/|L_p|$ should be satisfied to allow a positive $\bar{\tau}^l$. The choice of β presents us with several tradeoffs. While a smaller β decreases queueing delays in network, a larger β increases the utilization of the link capacity and alleviates the saturation effect at $q^l(t) = 0$. Here we argue that β should be set to the lowest value avoiding severe underutilization of the link capacity. One crucial reason for doing this is that $|L_p|$ can be arbitrarily large in real networks. Moreover, minimizing queueing delays is more important for many flows such as web traffic and multimedia traffic flows, and a higher β increases

$\bar{\tau}^l$ which is directly related to the performance of the network as shown in Eq. (3.30). In summary, we may use the following equation for selection of $\bar{\tau}^l$ and q_T^l .

$$\bar{\tau}^l = \frac{\tau_{prop_{p^*}}}{1 - |L_{p^*}|\beta} \quad \text{and} \quad q_T^l = \beta \bar{\tau}^l \mu^l \quad (3.32)$$

where $\tau_{prop_{p^*}}$ is the round-trip propagation delay on path p^* , $|L_{p^*}|$ is the number of links on the path p^* , and $p^* \in p_l$ is the round-trip path maximizing $\tau_{prop_{p^*}}/(1 - |L_{p^*}|\beta)$.

For the PII^2 model, $\bar{\tau}^l$ can be simply set to the maximum round-trip propagation delay among all paths traversing the link l , that is, $\beta = 0$. Finally, note that α_T^l in the PII^2 model might be lowered to decrease queues at transient period at the cost of less utilization.

3.5.2 Estimation of $|Q_w^l|$

To eliminate the overhead of storing per-flow information in a router, the sum of locally bottlenecked flows' weights, $|Q_w^l| = \sum_{i \in Q^l} w_i$, should be estimated. In general, we follow the method described in [7] and extend the method for *weighted max-min fairness property*. When the k th control packet arrives at link l at time t^j , it contains values of w_i , m_i and $a_i(t^j - \tau_i^{l,f})$. Using these values, for the k th interval, the sum of locally bottlenecked flows' weights can be *approximated* by

$$|\hat{Q}_w^l|^k = \sum_{t^j \in ((k-1)W, kW]} \frac{\text{DPS} \cdot \text{NCP} + \text{CPS}}{W \cdot a_i(t^j - \tau_i^{l,f})} \cdot w_i \cdot 1 \left\{ a_i(t^j - \tau_i^{l,f}) - m_i \geq \delta \cdot w_i f^l(t^j) \right\}$$

where $1 \{ \cdot \}$ is the indicator function, W is the time interval used for averaging, CPS is the control packet size. DPS is the average data packet size and it is assumed that for every transmission of $\text{DPS} \cdot \text{NCP}$ bytes, a source sends a control packet. The portion of control packets is $\text{CPS}/(\text{DPS} \cdot \text{NCP} + \text{CPS})$. The value $\delta = 0.9$ is used to introduce a margin for estimation. As we have shown in Theorem 3.2, it is safe to overestimate the sum of weights. For suppression of the fluctuation in estimation, the value $|\hat{Q}_w^l|$ is computed as follows:

$$|\hat{Q}_w^l| \leftarrow \lambda |\hat{Q}_w^l| + (1 - \lambda) |\hat{Q}_w^l|^k$$

where λ is an averaging factor and it is found that λ yields the stable and effective estimation of $|\hat{Q}_w^l|$ when it is set to $\lambda = 0.98$.

3.5.3 Discrete-Time Implementations

Our proposed fluid models must be discretized to smooth out the high-frequency fluctuation of $e_1^l(t)$ and $e_2^l(t)$, noisy variation of $f^l(t)$ caused by packet-to-packet fluctuation and background traffic fluctuation. A recommended implementation of the PID model for the computation of $f^l(t)$ with a sampling time T_1 is given by

$$f^l[k] = \left[f^l[k-1] - \frac{1}{|\hat{Q}_w^l| + w_{max}} \left(A(e_1^l[k] - e_1^l[k-1]) + BT_1 e_1^l[k] + \frac{C}{T_1} (e_1^l[k] - 2e_1^l[k-1] + e_1^l[k-2]) \right) \right]_0^{\bar{\mu}^l} \quad (3.33)$$

where $A = G_P/\bar{\tau}^l > 0$, $B = G_I/(\bar{\tau}^l)^2 > 0$, $C = G_D \geq 0$, and the saturation function is defined as $[\cdot]_0^{\bar{\mu}^l} = \min[\max[\cdot, 0], \bar{\mu}^l]$. An integrated version of Eq. (3.33) seems infeasible because $-BT_1 \sum_{i=0}^k e_1^l[i]$ goes to infinity as k goes to infinity for underloaded links where $q[\cdot] = 0$. One possible choice of antialiasing filter of $q^l(t)$ is using periodic-averaging filter, i.e., $e_1^l[k] = \frac{1}{T_1} \int_{(k-1)T_1}^{kT_1} q^l(t) dt - q_T^l$. The value w_{max} is the maximum value of weights, $w_{max} \equiv \max_{i \in N} w_i$, which is added to avoid underestimation of $|Q_w^l|$ when a flow with a weight value of w_{max} arrives at links.

For the PII^2 model, a recommended implementation for computation of $f^l(t)$ is given by

$$f^l[k] = \left[2f^l[k-1] - f^l[k-2] - \frac{1}{|\hat{Q}_w^l| + w_{max}} \left(AT_2(e_2^l[k] - e_2^l[k-1]) + BT_2^2 e_2^l[k] + C(e_2^l[k] - 2e_2^l[k-1] + e_2^l[k-2]) \right) \right]_0^{\alpha_T^l \mu^l}$$

where $A = H_I/\bar{\tau}^l > 0$, $B = H_{I^2}/(\bar{\tau}^l)^2 > 0$, $C = H_P \geq 0$. One choice of $e_2^l[k]$ is $e_2^l[k] = \frac{1}{T_2} q^{l+}[k] - \alpha_T \mu$ where $q^+[k]$ is the byte sum of packets enqueued during the time interval $((k-1)T_2, kT_2]$.

3.6 Simulation Results

Here we give simulation results in two scenarios to demonstrate the performance of our algorithms and to compare the performance of two models. The simulations are done using the ns-2 simulator [32]. To be more realistic, the maximum round-trip distance is set to the distance round the earth, which is about $4 \times 10^4 \text{ km}$ in all two scenarios. Thus the largest

Table 3.1: Parameters Used for Simulation.

$\bar{\mu}^l$	β	T_1	α_T^l	T_2	δ	λ	CPS	DPS	NCP	W
$1.1\mu_l$	0.02	30Δ	0.95	150Δ	0.9	0.98	40bytes	500bytes	30	300Δ

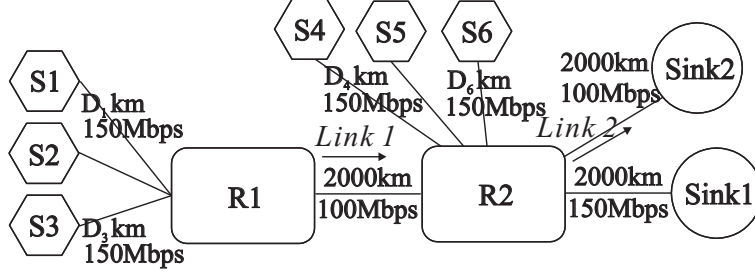


Figure 3.6: Multiple bottleneck network used for Scenario 1

round-trip propagation delay on paths traversing a link is set to $\tau_{prop_p^*} = 200\text{ms}$ with the signal propagation speed of $2 \times 10^5 \text{km/s}$ and $\bar{\tau}^l = 200\text{ms}/(1 - |L_{p^*}|\beta)$ is used for the PID model and $\bar{\tau}^l = 200\text{ms} + \tau_{marg}$ is used for the PII² model. $\tau_{marg} = 20\text{ms}$ is introduced to compensate the discretization delay of T_2 . The value of $|L_{p^*}|$ is set to 4 and 2 respectively in scenario 1 and 2, assuming that the links of sources and sinks do not incur queueing delays. We assume that all packets are enqueued in the same buffer and served simply with FCFS discipline and w_{max} is set to 3. Other parameters used for simulation are given in Table 3.1 where Δ is one data packet transmission time, i.e., $\Delta \equiv \text{DPS}/\mu^l$. Note that the target queue lengths are $q_T^l \approx 50\text{kbytes}$ with $\mu^l = 100\text{Mbps}$ and the queueing delay of a link with $q^l(t) = q_T^l$ is approximately 4ms for the PID model. The portion of control packets is 0.266%. Simulation results for PID, PII², PI and II² models are respectively denoted by G_{PID}^3 , $G_{PII^2}^3$, G_{PID}^2 and $G_{PII^2}^2$.

3.6.1 Scenario 1: Multiple Bottleneck Network With Heterogeneous Round-Trip Delays

In the first scenario, we investigate various properties of our algorithm. In [27], authors showed through simulations that the local stability condition derived in the neighborhood works well for the FCFS discipline. Two assumptions, remotely-throttled-first-serve (RTFS) and weighted sharing discipline, were needed to decouple the dynamics of the multiple bot-

Table 3.2: Flow Models Used for Scenario 1 and Fair Rate. (The units of m_i and Fair rate are in Mbps and the units of D_i are in km. The units of Arrival and Departure time are in seconds.)

Src.	m_i	w_i	D_i	Arr.	Dept.	Sink
S1	5(4.75)	1	8000	$-\infty$	∞	Sink1
S2	15(14.25)	3	16000	$-\infty$	∞	Sink1
S3	0	2	4000	5	∞	Sink2
S4	20(19)	3	8000	$-\infty$	∞	Sink2
S5	0	3	12000	$-\infty$	20	Sink2
S6	0	2	4000	10	15	Sink2

Src.	Fair Rate in Time Interval				
	$-\infty \sim 5$	$5 \sim 10$	$10 \sim 15$	$15 \sim 20$	$20 \sim \infty$
S1	25(23.75)	20(19)	21(19.95)	20(19)	18.33(17.42)
S2	75(71.25)	60(57)	63(59.85)	60(57)	55(52.25)
S3	-	20(19)	16(15.2)	20(19)	26.67(25.3)
S4	60(57)	50(47.5)	44(41.8)	50(47.5)	73.33(69.7)
S5	40(38)	30(28.5)	24(22.8)	30(28.5)	-
S6	-	-	16(15.2)	-	-

tleneck networks mathematically. They also showed through simulations that FCFS works better than RTFS. By appealing to this result, we here consider a scenario where two bottlenecks exist. The network configuration is shown in Fig. 3.6 where the bottleneck links 1 and 2 have the link capacity of 100Mbps. The flow models used in this scenario and theoretical rates of flows satisfying the *weighted max-min fairness property* for the PID model are summarized in Table 3.2. For the PII^2 model, changes are indicated in parentheses when needed.

At $t = 0s$, the queue lengths at link 1 and 2 are already stabilized with 4 flows, S1, S2, S4 and S5. For four gain sets, values of $q^l(t)$ and $|\hat{Q}_w^l|$ at link 1 and 2, and source transmission rates $a_i(t)$ are shown in Fig. 3.7. For G_{PID}^3 and G_{PID}^2 , the queue lengths are controlled to the target queue length except transient periods. For $G_{PII^2}^3$ and $G_{PII^2}^2$, the

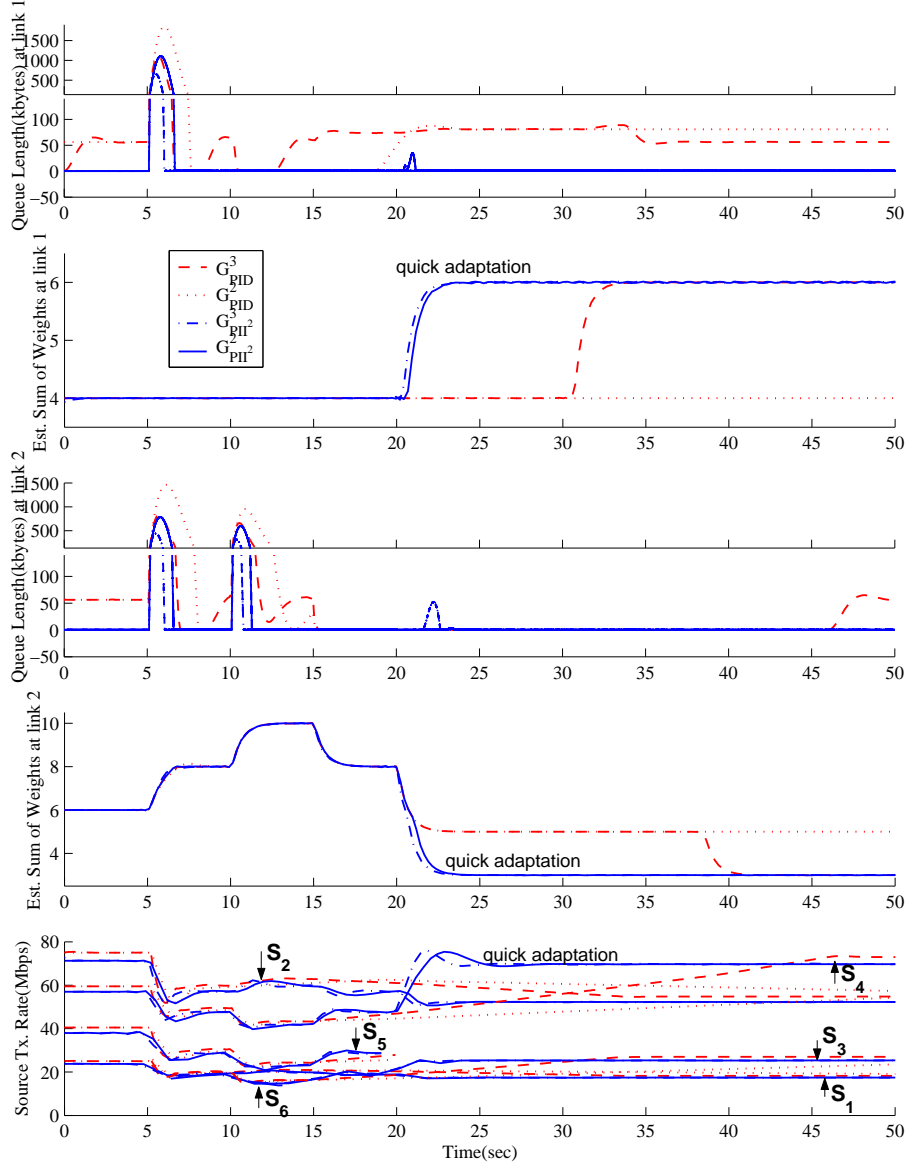


Figure 3.7: Results of Scenario 1: From top to bottom - Queue length at links 1 ($q^1(t)$), Estimated sum of locally bottlenecked flows' weights at link 1 ($|\hat{Q}_w^1|$), Queue length at link 2 ($q^2(t)$), Estimated sum of locally bottlenecked flows' weights at link 2 ($|\hat{Q}_w^2|$) and Source Transmission Rates ($a_i(t)$).

queue lengths are nearly zero except transient periods, at the cost of 5% underutilization. It can be observed that the queue length overshoot is smaller and the rate adaptation is faster when a three-term controller (G_{PID}^3 or $G_{PII^2}^3$) is used instead of a two-term controller (G_{PID}^2 or $G_{PII^2}^2$). The overshoots of queue length at $t = 5s$ and $t = 10s$ are mainly due to the smallness of $|Q_w^l|$ in this scenario. When $|Q_w^l|$ becomes large, $|Q_w^l| \gg 1$, such overshoots can be reduced. At $t = 50s$, the queue length with the gain set G_{PID}^2 is still being stabilized after the departure of S5 at $t = 20s$ because the error signal $e_1^2(t)$ is saturated to $-q_T^l$ due to the saturation nonlinearity at $q^2(t) = 0$. $G_{PII^2}^3$ and $G_{PII^2}^2$ achieve theoretical fair rates in advance of two gain sets used for the PID model. S3 is bottlenecked at link 2 from $t = 5s$ to $t = 20s$ and bottlenecked at link 1 as S5 stops its transmission at $t = 20s$. The actual source transmission rates approach to the theoretical fair rates given in Table 3.2 except transient period. We can see that our algorithms work well even if multiple bottlenecks exist.

3.6.2 Scenario 2: Simple Network With Short-lived Flows

In the second scenario, we investigate the effect of short-lived flows to our algorithm. We use a simple network shown in Fig. 3.8 where 10 persistent sources with $D_i = i \times 1800\text{km}$, $i \in \{1, 2, \dots, 10\}$ and 15 on-off sources with $D_i = (i - 10) \times 1200\text{km}$, $i \in \{11, 12, \dots, 25\}$ exist. A on-off source is modelled by a two-state birth-death model where the dwell time periods in on and off states are exponentially distributed with the mean of 5s and 10s respectively. $w_i = 1$ and $m_i = 0$ are used. A portion of the simulation results is shown in Fig. 3.9. Although the results are oscillatory due to short-lived flows, the feedback rate and estimated sum of flows' weights at link 3 are kept in the neighborhood of 6.67Mbps(or 6.33Mbps) and 15 respectively. Note that the PII^2 model is good at tracking ideal fair rates and $G_{PII^2}^3$ has the smallest transient queue length. The utilization of link 3 is found to be 0.946, 0.913, 0.947 and 0.945 respectively with the gain set G_{PID}^3 , G_{PID}^2 , $G_{PII^2}^3$ and $G_{PII^2}^2$. The low utilization of G_{PID}^2 is caused by its slow rate adaptation when the queue length is zero. The utilization of $G_{PII^2}^3$ and $G_{PII^2}^2$ is very close to $\alpha_T^3 = 0.95$ due to their fast rate adaptation.

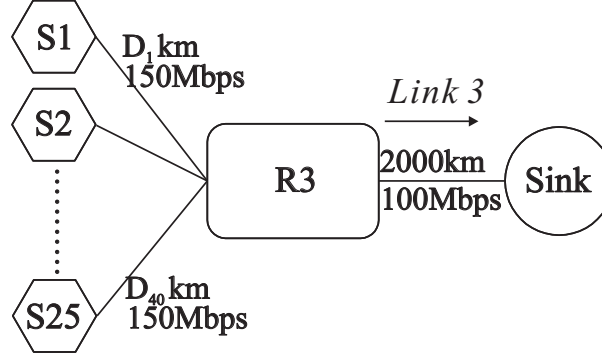


Figure 3.8: Simple network used for Scenario 2.

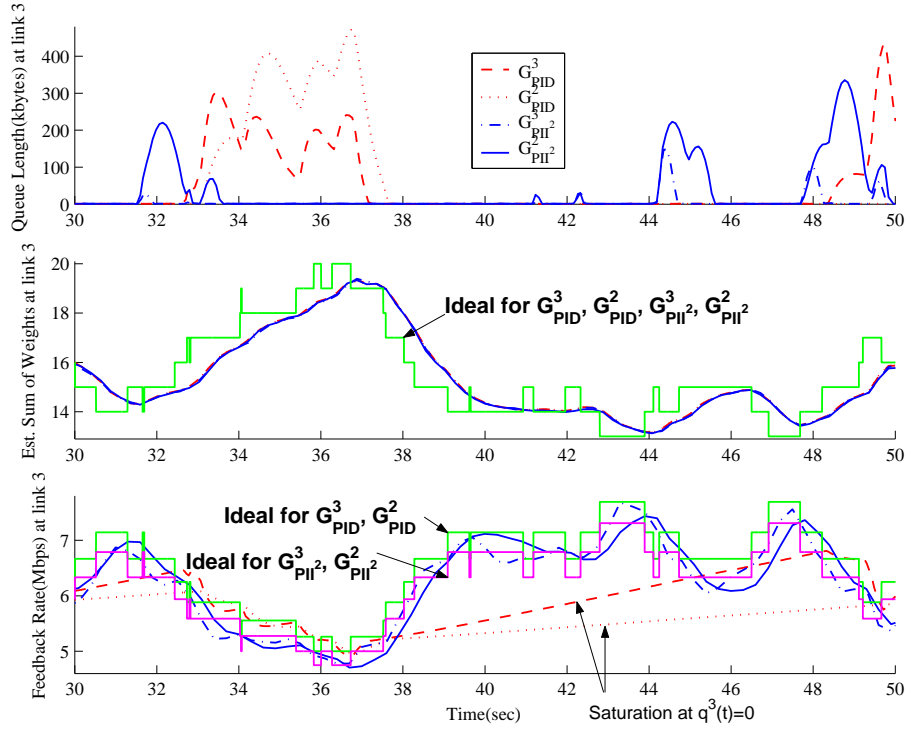


Figure 3.9: Results of Scenario 2: From top to bottom - Queue length at link 3 ($q^3(t)$), Estimated sum of locally bottlenecked flows' weights at link 3 ($|\hat{Q}_w^3|$) and Feedback rate at link 3 ($u^3(t)$).

CHAPTER 4

APPLICATION-PERFORMANCE ORIENTED FLOW CONTROL

4.1 Introduction

One of the most common understandings of fairness for a best-effort service network is *max-min fairness* as defined in [1]. An easy algorithm for obtaining a max-min fair allocation, which is also known as a *water-filling* algorithm, is given in [1, 33]: rates of flows are increased at the same pace until a link is saturated. Then the rates of flows passing through the saturated link are fixed and others continue to increase at the same pace. (In this paper, we do not deal with other concepts of fairness [2, 12–14].)

There are several works [7, 20, 22, 27] that provide distributed and stable max-min flow control algorithms that work in single and multiple bottleneck networks in spite of round-trip delays. Recently, Radunović and LeBoudec [33] pointed out that there are some cases to which the notion of a bottleneck link and the water-filling approach is not applicable. They considered not only max-min, but also min-max, fairness and observed that the existence of max-min fairness is actually a geometric property of the set of feasible allocations. Based on the relation between max-min fairness and leximin ordering, they completed a unified framework encompassing weighted and unweighted max-min fairness, and utility max-min fairness (to be explained) and provided a centralized algorithm that yields these fairness properties.

In a single link case, utility max-min corresponds to the satisfaction (utilities) of each user in the network being equal. Let us consider a simple network in which a link of capacity

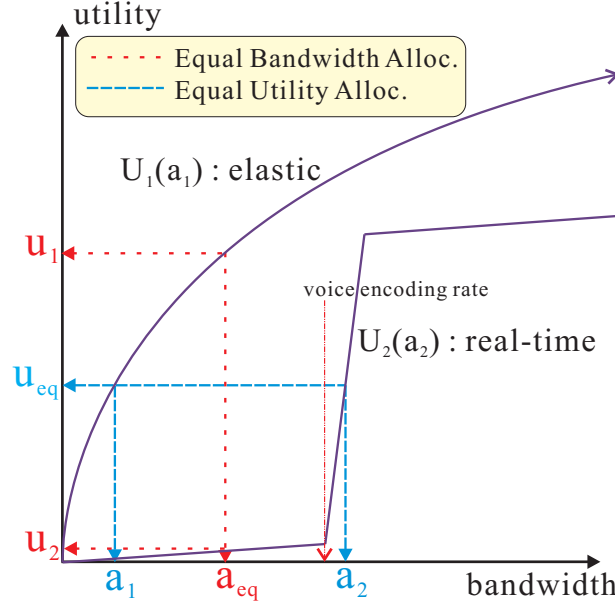


Figure 4.1: Bandwidth max-min fairness versus utility max-min fairness.

μ is shared by two flows: an elastic flow with utility function $U_1(\cdot)$ and a real-time flow that transfers voice data with utility function $U_2(\cdot)$. As shown in Fig. 4.1, if the link capacity is shared equally (i.e., $a_{eq} = \frac{\mu}{2}$), the utility of the elastic flow, $u_1(= U_1(a_{eq}))$, becomes much larger than that of the real-time flow, $u_2(= U_2(a_{eq}))$, and the real-time flow is unsatisfactory because the allowed rate is smaller than the voice encoding rate. In contrast, if the link capacity is shared in a way that $U_1^{-1}(u_{eq}) + U_2^{-1}(u_{eq}) = \mu$, then both flows gain an identical utility (i.e., $U_1(a_1) = U_2(a_2) = u_{eq}$), and the real-time flow is satisfied with the allocation because the allowed rate is greater than the voice encoding rate. The former represents the bandwidth max-min fair allocation (equal bandwidth allocation in the single link case) whereas the latter represents the utility max-min fair allocation (equal utility allocation in the single link case).

There are several works [16, 23, 33] that present link algorithms to achieve the utility max-min fair bandwidth allocation, assuming that each link knows the utility functions of all the flows sharing the link. Note that the algorithms used in the cited studies are not distributed in the strict sense because they require global information, such as utility functions of users. Questions remain: (i) whether or not there exists a *distributed* link

algorithm that does not require per-flow information, including utility function information, and (ii) whether or not such an algorithm converges in the presence of round-trip delays. As a solution to these questions, we provide a network architecture with a distributed flow control algorithm that achieves utility max-min fairness without using any kind of per-flow operations and provide stability results for the proposed flow control algorithm. In our proposed architecture, links do not need to know the utility functions of flows sharing the links.

Wyrowski et al. [28] proposed a somewhat similar architecture, although they did not mention utility max-min fairness. They considered a *linearized model* in which even gain values depend on the equilibrium point, which cannot be known in advance. Note that utility functions are naturally nonlinear and local stability results obtained through linearization techniques cannot guarantee global stability. It is very difficult to find a *region of attraction* [21] in such works. In contrast to this work, we consider a *nonlinear model* that does not exploit knowledge of the equilibrium point. To the best of our knowledge, this is the first work dealing with an analytical framework for the original problem and its stability.

The definition of utility max-min fairness is similar to that of bandwidth max-min fairness, except that utility values of users are max-min fair. Let us denote flow i 's utility value and utility function by u_i and $U_i(\cdot)$, respectively. Two technical assumptions on $U_i(\cdot)$ for the analysis of the proposed network architecture are given as follows:

- A.1. We assume that $U_i(\cdot)$ is a continuous and increasing function of user i 's allocated data rate. By this assumption there always exists an inverse function of $U_i(\cdot)$, i.e., $U_i^{-1}(\cdot)$. It is quite natural that the values of utility functions increase as the allocated data rates increase.
- A.2. We assume that $U_i(0) = 0$. It is also quite reasonable, since the utility function value of user i , i.e., the degree of user i 's satisfaction, is zero when zero data rate is allocated.

Let us denote the set of all links, the set of all flows and the set of flows traversing link l by L , N and $N(l)$, respectively. Their cardinalities are denoted by $|L|$, $|N|$ and $|N(l)|$, respectively. Then, similar to the bandwidth max-min fairness [1], the utility max-min fairness can be defined as follows.

Definition 4.1: A rate vector $\langle a_1, \dots, a_{|N|} \rangle$ is said to be *feasible* if it satisfies $a_i \geq 0$, $\forall i \in N$ and $\sum_{i \in N(l)} a_i \leq \alpha_T^l \mu^l$, $\forall l \in L$.

Definition 4.2: A rate vector $\langle a_1, \dots, a_{|N|} \rangle$ is said to be *utility max-min fair* if it is feasible, and for each $i \in N$ and feasible rate vector $\langle \bar{a}_1, \dots, \bar{a}_{|N|} \rangle$ for which $U_i(a_i) < U_i(\bar{a}_i)$, there exists some i' with $U_i(a_i) \geq U_{i'}(a_{i'}) > U_{i'}(\bar{a}_{i'})$.

Here μ^l denotes the capacity of link l and α_T^l is a constant defining target link utilization of link l ($0 < \alpha_T^l \leq 1$). Let a vector $\langle u_1, \dots, u_{|N|} \rangle$ denote the utility vector corresponding to the rate vector $\langle a_1, \dots, a_{|N|} \rangle$ where $u_i = U_i(a_i)$, $\forall i \in N$. Then, Definition 4.2 can be restated more informally as follows: a rate vector $\langle a_1, \dots, a_{|N|} \rangle$ is said to be utility max-min fair if it is feasible and for each user $i \in N$, its utility u_i cannot be increased while maintaining feasibility without decreasing the utility $u_{i'}$ for some user i' for which $u_{i'} \leq u_i$.

4.2 Motivation and Backgrounds for Absolute Stability

4.2.1 Motivation

In Chapter 3, we have proposed two network models using PID (proportional, integral, derivative) and PII² (proportional, integral, double integral) link controllers and proved the asymptotic stability of the closed-loop systems with Nyquist stability criterion [25] and Zero exclusion theorem in robust control theory [26, 29] when flows experience heterogeneous round-trip delays. We also have shown that PID and PII² link controller models are identical in the sense that open-loop transfer functions are identical and stability region for gains is identical. Compared with PID model, it is shown that PII² model converges faster because there is no saturation of feedback control when router buffers are empty. Therefore, in this chapter, we concentrate on the PID model and avoid repetition regarding PII² model. In homogeneous-delay case where round-trip delays of all flows are equal to τ , the open-loop transfer function of PID link controller model was given by the following equation. (Eq. (3.11) in Section 3.3.1)

$$G(s) \triangleq \frac{g_P s + g_I + g_D s^2}{s^2} \exp(-\tau s). \quad (4.1)$$

We can find a stabilizing gain set (g_D, g_P, g_I) by choosing a gain set (G_D, G_P, G_I) residing in stability region depicted in Fig. 3.3 in Section 3.3.2 and calculate (g_D, g_P, g_I) using the

following relations.

$$G_D \triangleq g_D, \quad G_P \triangleq g_P \tau, \quad G_I \triangleq g_I \tau^2. \quad (4.2)$$

For heterogeneous-delay case, denoting by $\bar{\tau}$, an upper bound of τ_i s, we also can find a stabilizing gain set (g_D, g_P, g_I) by choosing a gain set (G_D, G_P, G_I) and using $\bar{\tau}$ instead of τ in Eq. (4.2).

We can see that this system can be regarded as a feedback connection of a linear system $G(s)$ and an identical function, i.e., $\phi(y) = y$. If $\phi(\cdot)$ can be replaced by a memoryless nonlinear function $\phi^*(\cdot)$ satisfying some conditions while the asymptotic stability still holds, we can expect that some kind of utility functions related to $\phi^*(\cdot)$ may be employed for utility max-min architecture. The problem of finding stability condition for this kind of nonlinear feedback systems has received much attention in *absolute stability* literature.

4.2.2 Backgrounds for Absolute Stability

If it were possible to deduce the stability of a family of nonlinear systems by examining only all linear systems within that family, then we may be relieved of burdens to analyze stability of nonlinear feedback systems. The history of absolute stability began with the tempting conjecture given by Aizerman [34]. Suppose $\phi(\cdot)$ is a time-invariant nonlinearity. His conjecture was that a linear system $G(s)$ with any nonlinear feedback $\phi(\cdot)$ *belonging to the sector* $[a, b]$, i.e., $ay \leq \phi(y) \leq by$, is asymptotically stable if $\phi(y) = ky$ for any k in $[a, b]$ stabilizes the given system. Two examples of $\phi(\cdot)$ belonging to the sector $[a, b]$ are shown in Fig. 4.2. Although this conjecture is fascinating, it is shown that this conjecture is false in general. But, inspired by this conjecture, there have appeared several criteria, e.g., Circle criterion and Popov criterion [21, 35], which can rigorously determine the stability of nonlinear feedback systems with graphical analysis.

Kalman made another conjecture [36] assuming a more stringent condition for $\phi(\cdot)$. Suppose $\phi(\cdot)$ is a memoryless time-invariant nonlinearity, and is continuously differentiable. His conjecture was that a linear system $G(s)$ with any nonlinear feedback $\phi(\cdot)$ belonging to the sector $[a, b]$, i.e., $ay \leq \phi(y) \leq by$, is asymptotically stable if $\phi(\cdot)$ *belongs to the incremental sector*, i.e., $\phi(0) = 0$ and $a \leq d\phi(y)/dy \leq b$. Although this conjecture is also shown to be false in general, due to the stringent assumption on $\phi(\cdot)$, its applicability can be higher. For more precise statements of two conjectures, readers are encouraged to

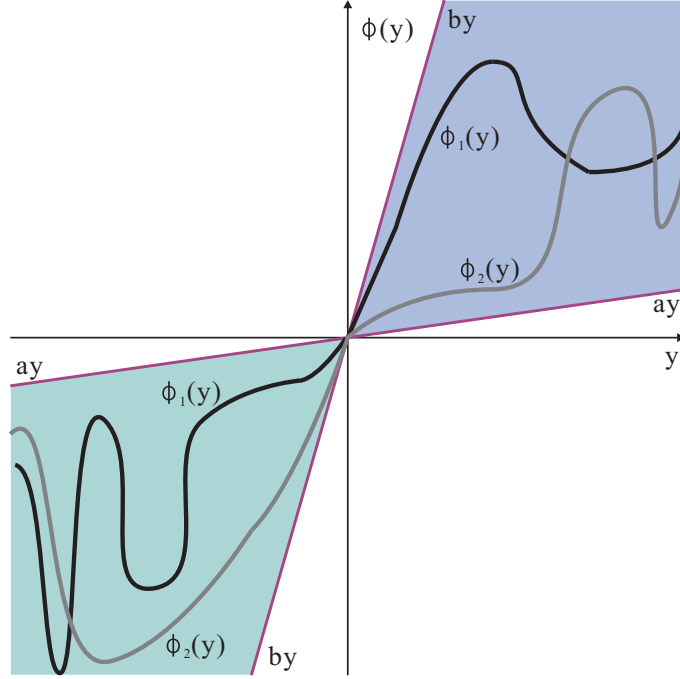


Figure 4.2: Two examples of $\phi(\cdot)$ belonging to the sector $[a, b]$.

refer to [21, 35].

We have several problems in applying absolute stability criteria to our network architecture. Although there is abundant literature including Circle criterion and Popov criterion, most of them assume that target systems have no delay and are based on Lyapunov function method and hence, are not applicable to delayed-systems. The second problem is that many criteria are quite restrictive which means that the shape of $\phi(\cdot)$ is quite limited and we are allowed to use only a narrow family of utility functions. The third problem is that they assume that the function $G(s)$ is asymptotically stable without a feedback; which is not the case for our systems. In view of aforementioned issues, the proposed system is changed to an asymptotically stable system $\bar{G}(s) (\neq G(s))$ having a nonlinear feedback connection, and then we apply Dewey and Jury's criterion [37] that is not based on Lyapunov function method.

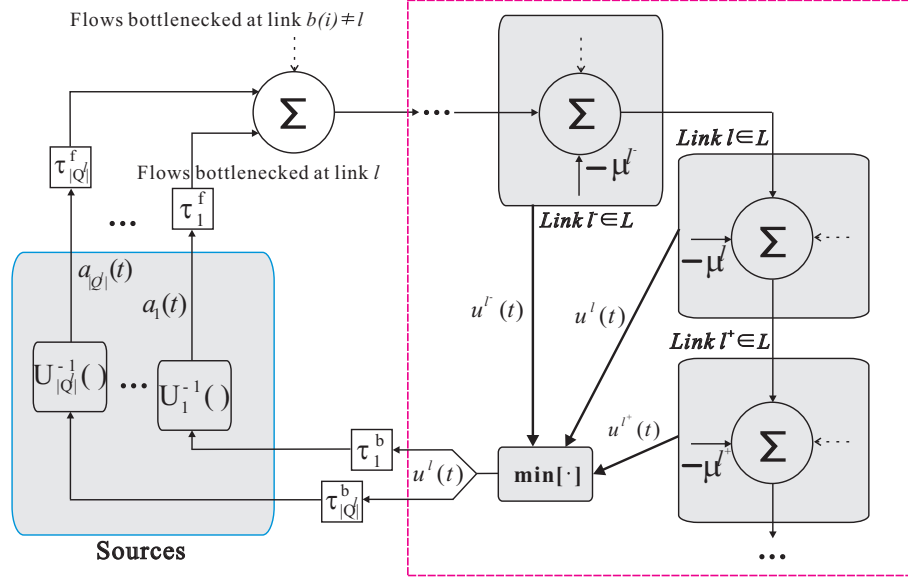


Figure 4.3: The network architecture for utility max-min fairness.

4.3 Utility Max-Min Architecture

In this section, we propose a network architecture that achieves utility max-min fairness at equilibrium. The network architecture with multiple sources and links is depicted in Fig. 4.3. Let us consider a bottleneck link $l \in L$. Then, the dynamics of the buffer of the link can be written as

$$\dot{q}^l(t) = \begin{cases} \sum_{i \in N(l)} a_i(t - \tau_i^{l,f}) - \mu^l, & q^l(t) > 0 \\ \left[\sum_{i \in N(l)} a_i(t - \tau_i^{l,f}) - \mu^l \right]^+, & q^l(t) = 0 \end{cases} \quad (4.3)$$

where $a_i(t)$ is the sending rate of source i , $\tau_i^{l,f}$ is the forward-path delay from source i to link l , μ^l is the link capacity of the link and the saturation function $[\cdot]^+ \triangleq \max[\cdot, 0]$ is such that the $q^l(t)$ cannot be negative.

A source i sends packets according to fair utility value assigned by the network. To achieve utility max-min fairness, let us assume that the source sends packets according to the minimum utility value among the utility values assigned by the links along the path of

its flow. Thus we assume the following *source algorithm*.

$$\textbf{Source Algorithm: } a_i(t) = U_i^{-1} \left(\underbrace{\min_{l \in L(i)} [u^l(t - \tau_i^{l,b})]}_{u_i(t)} \right), \quad (4.4)$$

where $L(i)$ is the set of links which flow i traverses, $u^l(t)$ is the utility value assigned by link l on the path of flow i , $\tau_i^{l,b}$ is the backward-path delay from link l to source i and $U_i(\cdot)$ is the user-specific utility function of user i . Because the $\min[\cdot]$ operation is taken over a finite number of links, there should exist at least one link l such that $u^l = \min[\cdot]$. Therefore, each flow i has at least one bottleneck $l \in L(i)$.

There are two assumptions employed for the analysis of the network model.

- D.1. We assume that the sources are *persistent* until the closed-loop system reaches a steady state. By persistent, we mean that the source always has enough data to transmit at the allocated rate.
- D.2. Two delays, say, the forward-path delay $\tau_i^{l,f}$ and the backward-path delay $\tau_i^{l,b}$, include propagation, queueing, transmission and processing delays. We denote the sum of two delays by τ_i and assume that this is constant.

4.3.1 PID and PII² Link Controller Models

To control flows and to achieve utility max-min fairness, we use a PID link controller at each link. In PID the link controller model, there is a specified target queue length q_T^l to avoid underutilization of the link capacity. Because we have a nonzero target queue length q_T^l , the PID model implies that $\alpha_T^l = 1$ in Definition 4.1. Each link calculates the common feedback utility value $u^l(t)$ for all flows traversing the link according to the PID control mechanism.

In general, a proportional term increases the convergence speed of transient responses and reduces errors caused by disturbances. An integral term can effectively eliminate steady state error and results in the size of the stability region being reduced. A derivative term adds some damping and extends the area of the stability region. It also improves the performance of the transient period.

Let us denote the set of flows bottlenecked at link l and its cardinality by Q^l and $|Q^l|$, respectively. The *link algorithm with PID controller* that uses the difference between $q^l(t)$ and q_T^l as input is given by the following equation

$$\textbf{Link Algorithm 1: } u^l(t) = \left[-\frac{1}{|Q^l|} \left(g_P e_1^l(t) + g_I \int_0^t e_1^l(t) dt + g_D \dot{e}_1^l(t) \right) \right]^+ \quad (4.5)$$

where $e_1^l(t) \triangleq q^l(t) - q_T^l$ is the error signal between control target and current output signal and, $g_P > 0$ and $g_I, g_D \geq 0$. It should be noted that we also can use a PII^2 controller as we did in Section 3.2.2, by defining $e_2^l(t) \triangleq \sum_{i \in N(l)} a_i(t - \tau_i^{l,f}) - \alpha_T^l \mu^l$ where $\alpha_T^l < 1$. The *link algorithm with PII^2 controller* is given by the following equation

$$\textbf{Link Algorithm 2: } u^l(t) = \left[-\frac{1}{|Q^l|} \left(h_P e_2^l(t) + h_I \int_0^t e_2^l(t) dt + h_{I^2} \int_0^t \int_0^t e_2^l(t) dt dt \right) \right]^+. \quad (4.6)$$

This model control flows so that the queue length at steady state becomes zero at the cost of link underutilization. The main advantage of this model is that the feedback signal is not saturated at $q^l(t) = 0$ and it is shown through simulations in Section 3.6 that the PII^2 model results in faster convergence. In this chapter, though we focus on the PID model to avoid repeating similar arguments for the PII^2 model, readers should note that one can derive similar arguments regarding the PII^2 model with ease, as was done in Chapter 3.

4.3.2 Steady State Analysis

Suppose that the closed-loop system has an equilibrium point at which the derivatives of the system variables are zero, i.e., $\lim_{t \rightarrow \infty} \dot{q}^l(t) = 0$, $\lim_{t \rightarrow \infty} q^l(t) = q_T^l$, $\lim_{t \rightarrow \infty} \dot{u}^l(t) = 0$, $\lim_{t \rightarrow \infty} u^l(t) = u_s^l$ and $\lim_{t \rightarrow \infty} a_i(t) = a_{is}$. More formally, the set of flows bottlenecked at link l is given by

$$Q^l = \{i \in N(l) \mid a_{is} = U_i^{-1}(u_s^l)\} \quad (4.7)$$

and the set of all flows not bottlenecked at link l but traversing link l , $N(l) - Q^l$, is given by

$$N(l) - Q^l = \{i \in N(l) \mid a_{is} = U_i^{-1}(u_s^{b(i)}) \text{ and } u_s^{b(i)} < u_s^l\}. \quad (4.8)$$

where $b(i) \in L(i)$ ($b(i) \neq l$) is some bottleneck for flow $i \in N(l) - Q^l$. Then the equation (4.3) implies that the link capacity μ^l in the PID link controller model is fully utilized as

follows:

$$\sum_{i \in N(l)} a_{is} = \mu^l. \quad (4.9)$$

Using Eq. (4.9), and the definitions (4.7) and (4.8), we obtain

$$\sum_{i \in Q^l} U_i^{-1}(u_s^l) + \sum_{i \in N(l) - Q^l} U_i^{-1}(u_s^{b(i)}) = \mu^l. \quad (4.10)$$

Thus, we finally get the following equation, which means that flows with utility values $u_s^{b(i)} < u_s^l$, which are not bottlenecked at link l , are assigned data rates $U_i^{-1}(u_s^{b(i)})$ in advance and the remaining capacity is fairly distributed to flows bottlenecked at link l based on the common utility value u_s^l .

$$U_i(a_{is}) = u_s^l = \left[\sum_{i \in Q^l} U_i^{-1} \right]^{-1} \left(\mu - \sum_{i \in N(l) - Q^l} U_i^{-1}(u_s^{b(i)}) \right)$$

for all $i \in Q^l$. From the above arguments, we can show that the proposed network architecture possesses the utility max-min fairness property. (The proof of Theorem 4.1 is in Appendix 6.5.)

Theorem 4.1 (Utility Max-Min Fairness): The proposed network architecture described by Eqs. (4.3), (4.4) and (4.5) (or (4.6)) achieves utility max-min fairness at steady state.

4.4 Stability Analysis

Although we presented a multiple bottleneck network model in Section 4.3.1, rigorous stability analysis of these kinds of models was shown to be very difficult in [27], due to the dynamics coupling among links that operate on a “first come first serve” (FCFS) principle. In [27], though such dynamics coupling exists in theory, the effect of coupling was shown to be negligible through various simulations. Recently, Wydrowski et al. [28] also showed that the dynamics coupling is of a very weak form. Thus, in this section, we drop the superscript l and the analysis is focused on a single bottleneck model. We conjecture that our analytical results can be extended to multiple bottleneck models without significant modification.

We provide a stability theorem when the saturation functions employed in Eqs. (4.3) and (4.5) are relaxed with a single bottleneck in the network. To overcome three theoretical

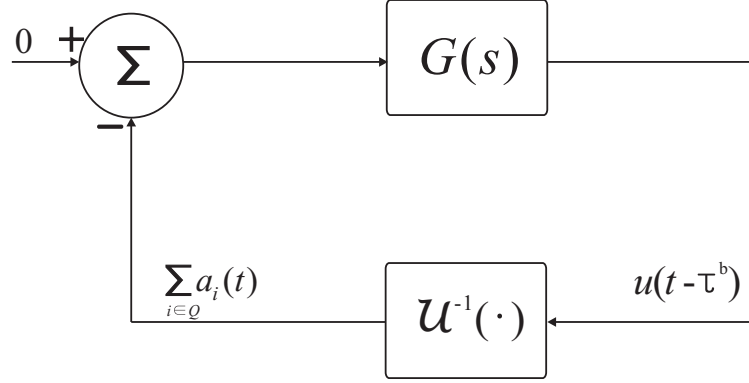


Figure 4.4: A block diagram of the proposed architecture.

difficulties pointed out in Section 4.2.2, we use a loop transformation and apply an improved absolute stability criterion to our system. Although our main stability theorem assumes that flows experience the same forward-path and backward-path delays, we conjecture that our theorem will hold even if flows experience heterogeneous delays, when an upper bound of τ_i s, i.e., $\bar{\tau} \geq \max_{i \in N} [\tau_i]$ is used.

4.4.1 Homogeneous-Delay Case

To analyze the homogeneous-delay case of the PID control model, let $\tau_i^f = \tau^f, \tau_i^b = \tau^b, \forall i \in Q$ and $\tau^f + \tau^b = \tau$. Then all flows experience the same forward-path and backward-path delay. By Eqs. (4.5) and (4.3), we obtain the following equation:

$$\ddot{u}(t - \tau^b) = -\frac{1}{|Q|} \left(\sum_{i \in Q} g_P \ddot{a}_i(t - \tau) + g_I \dot{a}_i(t - \tau) + g_D \ddot{a}_i(t - \tau) \right).$$

Thus we can see that the same transfer function $G(s)$ given in Eq. (4.1) defines the relationship between $-\sum_{i \in Q} a_i(t)$ and $u(t - \tau^b)$. By defining $\mathcal{U}(\cdot)$ as follows, we acquire the block diagram shown in Fig. 4.4 which is a feedback connection of $G(s)$ and an increasing and continuous nonlinearity $\mathcal{U}(\cdot)$.

$$\mathcal{U}^{-1}(u) \triangleq \frac{1}{|Q|} \sum_{i \in Q} U_i^{-1}(u). \quad (4.11)$$

Thus we can expect from Fig. 4.4 that an absolute stability theorem might be applicable to the proposed closed-loop system. Of various absolute stability criteria, we have found

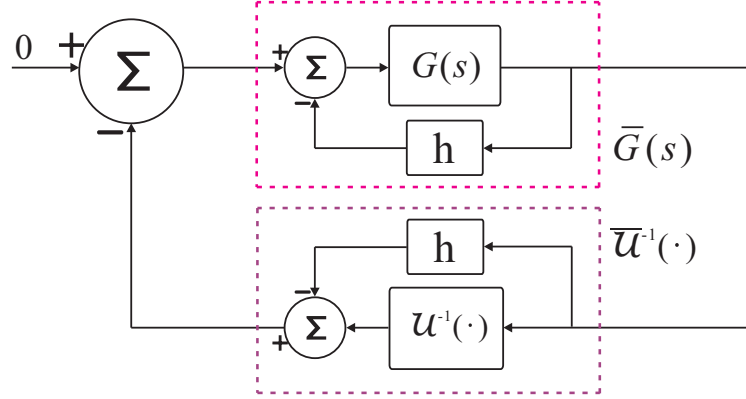


Figure 4.5: A block diagram of the proposed architecture after loop transformation.

that Dewey and Jury's criterion [37] is suitable for our systems based on arguments given in Section 4.2.2.

The first procedure when applying the criterion is to determine whether $G(s)$ is asymptotically stable because $G(s)$ itself without feedback is required to be asymptotically stable to apply the criterion. However, we can see that the transfer function $G(s)$ itself without feedback is not asymptotically stable because it has a double pole at $s = 0$. To overcome this problem, we use a loop transformation with a constant $h > 0$ and the resulting system is shown in Fig. 4.5. It should be noted that the modified system is identical to the original system. It is shown in Section 3.3.2 that the closed-loop system with feedback $\mathcal{U}^{-1}(u) = u$ (an identical function) is asymptotically stabilized when the gains $G_D \triangleq g_D$, $G_P \triangleq g_P\tau$ and $G_I \triangleq g_I\tau^2$ fall within a restricted area, shown in Fig. 3.3. Furthermore, it is also proven in Section 3.3.3 that the closed-loop system is asymptotically stable for any $|\hat{Q}_w| \geq |Q_w|$. ($|\hat{Q}_w|$ and $|Q_w|$ are defined in Section 3.3.3. In the systems of this chapter, it is assumed that $w_i = 1, \forall i \in Q$.)

To summarize, this result implies that the closed-loop system is asymptotically stable for $\mathcal{U}^{-1}(u) = hu, \forall h \in (0, 1]$ when we let $|\hat{Q}_w| = |Q_w|/h$. Hence we can see that $G(s)/(1 + hG(s))$ is asymptotically stable for any gain sets (G_D, G_P, G_I) falling within a restricted area shown in Fig. 3.3, and $h \in (0, 1]$. We are now ready to state the main result of this chapter. (Its proof is in Appendix 6.6.)

Theorem 4.2 (Homogeneous-Delay Case): The closed-loop system described by Eqs.

(4.3), (4.4) and (4.5) (or (4.6)) with the homogeneous-delay assumption $\tau_i^f = \tau^f, \tau_i^b = \tau^b$, $\forall i \in Q$ and $\tau = \tau^f + \tau^b$ is asymptotically stable for arbitrary utility functions with $0 < k \leq dU_i/da < \infty, \forall a \in [0, \infty)$ and $\forall i \in Q$ if a gain set (G_D, G_P, G_I) falls within a restricted area shown in Fig. 3.3 and there exist a finite number η and a finite number $\kappa \geq 0$ such that the open-loop transfer function $G(j\omega)$ satisfies the following equation for arbitrarily small $h > 0$:

$$\operatorname{Re} \left[\left(1 + \frac{j\omega\eta}{1 + \kappa\omega^2} \right) \frac{G(j\omega)}{1 + hG(j\omega)} \right] + k > 0, \quad \forall \omega \geq 0. \quad (4.12)$$

Remark 4.1: One should note that this requirement is not stringent because the maximum slopes of the utility functions are not restricted, except for the condition that they should not be infinite. In other words, this restriction means that a user's satisfaction should increase with minimum slope of k for the stability of the whole network. A user can sufficiently emphasize that his satisfaction increases significantly at a certain data rate with relatively high slope at that data rate; because what matters is not the absolute shape of one's utility function, but its relative shape compared with those of others.

The most effective aspect of this theorem is that utility functions have only the minimum slope requirement and one user can use an arbitrarily-shaped nonlinear utility function that may differ from the other users' utility functions. Note that we do not require any kinds of concavity assumptions which were required in previous approaches [2, 12–14]. We strongly believe that our requirement is one of the least restrictive and most practical requirements in utility max-min network architecture.

4.4.2 Graphical Interpretation of Theorem 4.2

We know from Section 3.3.1 that the closed-loop system is asymptotically stable when $U_i(a) = a$ for all $i \in N$. Thus we can infer that Theorem 4.2 is meaningful only when there exists $k \leq 1$ satisfying Eq. (4.12). Even though it is difficult to find a k satisfying Eq. (4.12) for general cases, the inequality admits an intuitive graphical technique similar to the Nyquist stability criterion [25]. Let us define two functions X and Y as follows:

$$X(\omega) \triangleq \operatorname{Re} \left[\frac{G(j\omega)}{1 + hG(j\omega)} \right], \quad Y(\omega) \triangleq \frac{\omega}{1 + \kappa\omega^2} \operatorname{Im} \left[\frac{G(j\omega)}{1 + hG(j\omega)} \right].$$

Then Eq. (4.12) is equivalent to the following condition:

$$X(\omega) - \eta Y(\omega) + k > 0, \forall \omega \geq 0 \iff \begin{pmatrix} 1 & -\eta \end{pmatrix} \begin{pmatrix} X(\omega) \\ Y(\omega) \end{pmatrix} > -k, \forall \omega \geq 0 \quad (4.13)$$

In two-dimensional Euclidean space, this inequality entails that the closed-loop system is asymptotically stable if there is a line with slope $1/\eta$ and an intercept on the X axis $-k$ such that $(X(\omega), Y(\omega))$ trajectory is completely contained in the open right half-space of the line. Because we have found that it is very difficult to find an equivalent and explicit symbolic expression of Eq. (4.12) independent of ω , we provide minimum values of k when two optimal gain sets found in Section 3.4 are used.

To find a k value independent of τ , we rewrite $G(j\omega)$, $X(j\omega)$ and $Y(j\omega)$ into the following equations using $\omega_1 \triangleq \tau\omega$ and relations given in Eq. (4.2).

$$G(j\omega_1) = -\frac{j\omega_1 G_P + G_I - \omega_1^2 G_D}{\omega_1^2} (\cos(\omega_1) - j\sin(\omega_1)),$$

$$X(\omega_1) \triangleq \operatorname{Re} \left[\frac{G(j\omega_1)}{1 + hG(j\omega_1)} \right], \quad Y(\omega_1) \triangleq \frac{\omega_1}{1 + \kappa'\omega_1^2} \operatorname{Im} \left[\frac{G(j\omega_1)}{1 + hG(j\omega_1)} \right].$$

where $\kappa' \triangleq \kappa/\tau^2$. (The proof of Corollary 4.1 is in Appendix 6.7.)

Corollary 4.1 (Explicit Range of k): For $G_{PID}^3 \triangleq (G_D, G_P, G_I) = (0.242, 0.868, 0.261)$ and $G_{PID}^2 \triangleq (G_D, G_P, G_I) = (0, 0.482, 0.091)$ that correspond to the PID and PI optimal gain sets, respectively, the minimum values of k are 0.480 and 0.338.

Remark 4.2: Note that, for $\kappa = 0$, Eq. (4.12) reduces to the well-known Popov criterion, and the minimum slope constraint is dropped. Fig. 4.6 shows that the minimum slope constraint in our theorem is essential for getting a smaller k . Thus, instead of the Popov criterion, which has been regarded as one of the least conservative criteria when the nonlinear feedback $\phi(\cdot)$ is time invariant, we must use Dewey and Jury's criterion, which allows much smaller values of k thanks to the minimum slope constraint.

This corollary provides minimum values of k for two optimal gain sets. For the PID and PI controller models, respectively, with the gain set G_{PID}^3 and G_{PID}^2 , we can use any kinds of utility function that satisfy, respectively, $0.480 \leq dU_i/da < \infty$ and $0.338 \leq dU_i/da < \infty$. To introduce stability margins to the closed-loop system, it is recommended that the minimum slopes of utility functions be bounded by 1.

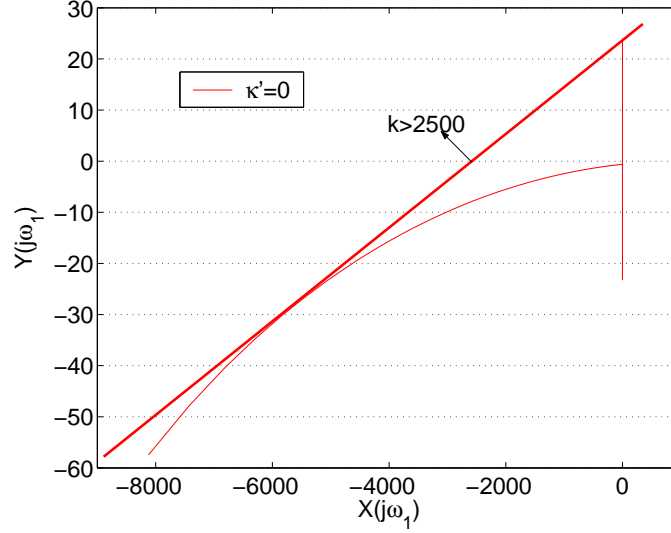


Figure 4.6: One sample of $(X(\omega_1), Y(\omega_1))$ plot for G_{PID}^3 with $h = 0.001$.

Lastly, we would like to comment on the *inevitability* of the minimum slope constraint in our distributed utility max-min architecture, represented by Eqs. (4.3), (4.4) and (4.5) (or (4.6)). In a single link case, Eq. (4.4) reduces to $a_i(t) = U_i^{-1}(u(t - \tau_i^b))$. If the slope dU_i/du is sufficiently small, a small change in $u(t)$ can induce a large fluctuation in $a_i(t)$. Since feedback delays between $a_i(t)$ and $u(t)$ are nonzero, the fluctuation of $a_i(t)$ is not alleviated immediately and causes the instability of the queue length through Eq. (4.3). Thus, we can see that the minimum slope constraint of utility functions is inevitable in a distributed utility max-min architecture with nonzero feedback delays.

4.5 Various Utility Functions

The utility function $U_i(\cdot)$ maps the bandwidth a_i , allocated by the network, to user i 's satisfaction. One question might arise as to how we can decide the shape of a utility function to make it represent application-specific satisfaction versus allocated bandwidth. In general, it is not an easy task to obtain a utility function of an application. Fortunately, there does exist a certain amount of research along these lines, as cited in [16]. To partially answer this question, we present four candidate utility functions in this section. We first define the

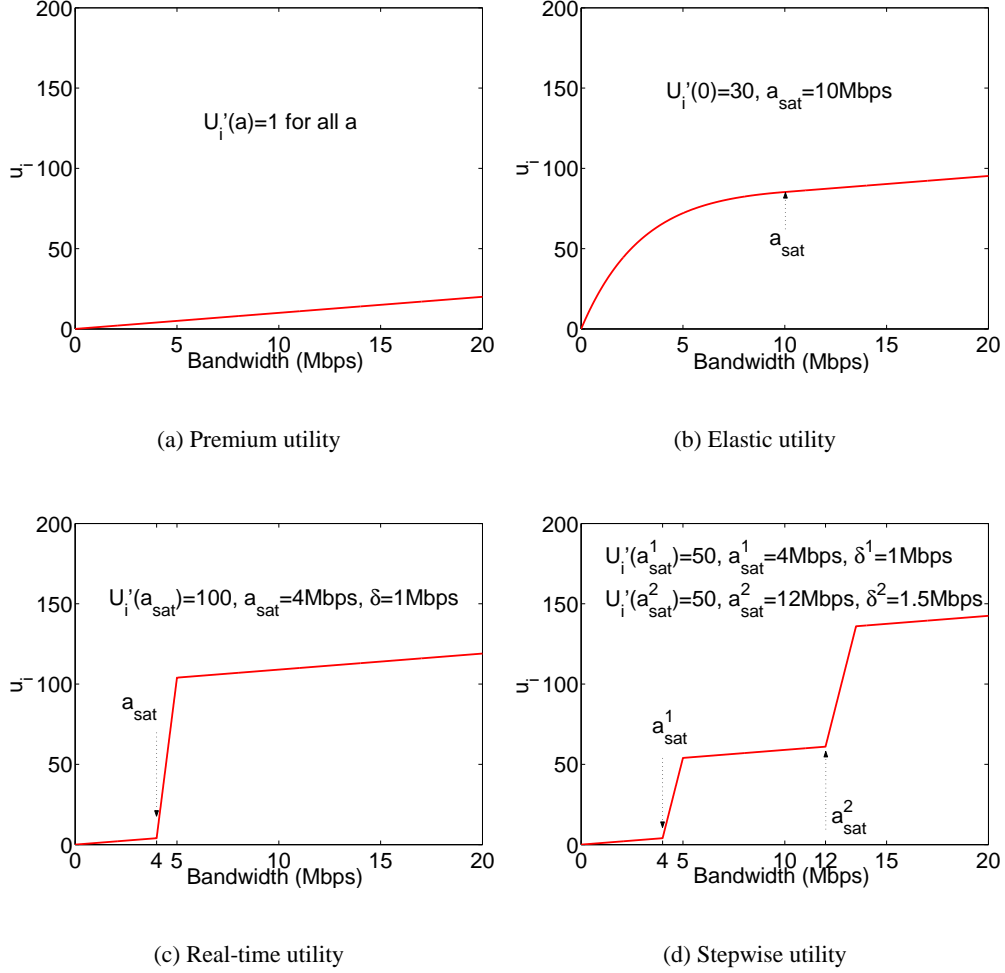


Figure 4.7: Utility functions for different application classes

premium utility where flows desire as much bandwidth as possible. In other words, premium flows yield the least satisfaction compared to other application flows when the same data rate is allocated to all flows. To satisfy the minimum slope constraint and to introduce stability margins, the premium utility is defined as $U_i(a) = a$ and shown in Fig. 4.7(a). It should be remarked that the value of $U_i(a)$ in Fig. 4.7 has no specific meaning and its unit can be arbitrarily chosen by introducing some scaling factor in Eqs. (4.5) and (4.6). What matters is the relative shape of utility functions, rather than utility values, as we mentioned

in Remark 4.1.

The *elastic utility* can be used for flows with elastic applications, such as FTP in the Internet. In this case, the satisfaction initially increases with a high slope followed by lower slopes when the allocated bandwidth exceeds a_{sat} . It is assumed that an elastic flow is satisfied sufficiently if $a \geq a_{sat}$. A candidate utility function using an exponential function is given by

$$U_i(a) = \begin{cases} k \left(1 - \exp\left(-\frac{U'_i(0)}{k}a\right) \right), & \text{if } a < a_{sat} \\ a - a_{sat} + k \left(1 - \exp\left(-\frac{U'_i(0)}{k}a_{sat}\right) \right), & \text{if } a \geq a_{sat} \end{cases}$$

where k is defined as $k \triangleq a_{sat}U'_i(0)/\log(U'_i(0))$. An elastic utility with $U'_i(0) = 30$ and $a_{sat} = 10\text{Mbps}$ is shown in Fig. 4.7(b). For a fixed value of a_{sat} , various values of $U'_i(0)$ result in different shapes of $U_i(\cdot)$. How can we choose $U'_i(0)$? One way to compare the absolute values of elastic utility to those of premium utility. In Fig. 4.7(a) and 4.7(b), when a premium flow is allocated 20Mbps, an elastic flow is allocated 0.8Mbps. When a premium flow is allocated 95.3Mbps, an elastic flow is allocated 20Mbps. Henceforth, one can choose an adequate value of $U'_i(0)$. The premium utility can be a *reference utility* for other utilities.

In this way, we provide a candidate for the *real-time utility*. A real-time flow would be unsatisfactory if the allowed rate is smaller than a specified rate a_{sat} . A real-time flow is satisfactory only when the allocated rate a is greater than or equal to a_{sat} . Thus, a candidate utility function is given by

$$U_i(a) = \begin{cases} a, & \text{if } a < a_{sat} \\ U'_i(a_{sat})(a - a_{sat}) + a_{sat}, & \text{if } a_{sat} \leq a < a_{sat} + \delta \\ a - \delta + U'_i(a_{sat})\delta, & \text{if } a \geq a_{sat} + \delta \end{cases}$$

A candidate function for real-time utility is shown in Fig. 4.7(c) with $U'_i(a_{sat}) = 100$, $a_{sat} = 4\text{Mbps}$ and $\delta = 1\text{Mbps}$. Compared to premium flows, a real-time flow is allocated at least 4Mbps when a flow with premium utility is allocated 4Mbps or more.

For multimedia flows with multi-layer streams where one layer is the base layer and the others are enhancement layers, the real-time utility can be extended to the *stepwise utility* where the application performance increases drastically when an additional streaming layer

is allocated to them. There are three variables $U'_i(a_{sat}^j)$, a_{sat}^j and δ^j , corresponding to each streaming layer. In the case of two streaming layers, a candidate utility function is given by

$$U_i(a) = \begin{cases} a & , \text{ if } a < a_{sat}^1 \\ U'_i(a_{sat}^1)(a - a_{sat}^1) + a_{sat}^1 & , \text{ if } a_{sat}^1 \leq a < a_{sat}^1 + \delta^1 \\ a - \delta^1 + U'_i(a_{sat}^1)\delta^1 & , \text{ if } a_{sat}^1 + \delta^1 \leq a < a_{sat}^2 \\ U'_i(a_{sat}^2)(a - a_{sat}^2) + a_{sat}^2 - \delta^1 + U'_i(a_{sat}^1)\delta^1 & , \text{ if } a_{sat}^2 \leq a < a_{sat}^2 + \delta^2 \\ a - \delta^2 + U'_i(a_{sat}^2)\delta^2 - \delta^1 + U'_i(a_{sat}^1)\delta^1 & , \text{ if } a \geq a_{sat}^2 + \delta^2. \end{cases}$$

A sample stepwise utility is shown in Fig. 4.7(d).

4.6 Implementation Considerations

4.6.1 Estimation of $|Q^l|$

The usage of $|Q^l|$, the number of flows bottlenecked at link l , in Eqs. (4.5) and (4.6) is not a specific requirement of our architecture but an inevitable requirement of most approaches. In most approaches, the gain value used for updating source rates or link prices is normalized by analogous terms. It should be noted that routers should store per-flow information regarding flows' activeness to know the exact value of $|Q^l|$. Thus, to eliminate this overhead, $|Q^l|$ must be estimated properly. The condition of Eq. (6.5) is still satisfied when $|Q|$ in Eq. (4.11) is replaced by $|\hat{Q}| \geq |Q|$. Thus, we can see that the overestimation of $|Q^l|$ is allowed, while severe overestimation slows down the convergence speed of the closed-loop system.

In general, we follow the method described in [7] and modify the method for utility max-min fairness. When the j th data packet arrives at link l at time t^j , it contains two fields, $a_i(t^j - \tau_i^{l,f})$ and $u^{l'}(t^j - \tau_i^{l',f})$ where l' is the current bottleneck link for flow i . Using these two values, for the k th interval, the number of flows bottlenecked at link l can be approximated by

$$|\hat{Q}^l|^k = \sum_{t^j \in ((k-1)W, kW]} \frac{\text{DPS}^j}{W \cdot a_i(t^j - \tau_i^{l,f})} \cdot 1 \left\{ u^{l'}(t^j - \tau_i^{l',f}) \geq \delta \cdot u^l(t^j) \right\} \quad (4.14)$$

where $1 \{ \cdot \}$ is the indicator function, W is the time interval used for averaging and DPS^j is the size of the j th data packet. When $u^{l'}(t^j - \tau_i^{l',f}) \geq \delta \cdot u^l(t^j)$, flow i is regarded a flow

bottlenecked at link l and the indicator function returns 1, otherwise 0. The value $\delta = 0.9$ is used to introduce a margin for estimation. Note that Eq. (4.14) provides an efficient method for estimating $|Q^l|$ in addition to preventing underestimation of $|Q^l|$. For suppression of the fluctuation in estimation, the value $|\hat{Q}^l|$ is computed as follows:

$$|\hat{Q}^l| \leftarrow \max[1, \lambda|\hat{Q}^l| + (1 - \lambda)|\hat{Q}^l|^k]$$

where λ is an averaging factor and it is found that λ yields the stable and effective estimation of $|\hat{Q}^l|$ when it is set to $\lambda = 0.98$.

4.6.2 Discrete-Time Implementations

Our proposed fluid models must be discretized to smooth out the high-frequency fluctuation of $e_1^l(t)$ and $e_2^l(t)$, noisy variation of $u^l(t)$ caused by packet-to-packet fluctuation and background traffic fluctuation. A recommended implementation of the PID model for the computation of $u^l(t)$ with a sampling time T_1 is given by

$$\begin{aligned} u^l[k] = & \left[u^l[k-1] - \frac{1}{|\hat{Q}^l|} \left(A(e_1^l[k] - e_1^l[k-1]) \right. \right. \\ & \left. \left. + BT_1 e_1^l[k] + \frac{C}{T_1} (e_1^l[k] - 2e_1^l[k-1] + e_1^l[k-2]) \right) \right]_{\bar{u}^l} \end{aligned} \quad (4.15)$$

where $A = G_P/\bar{\tau} > 0$, $B = G_I/\bar{\tau}^2 \geq 0$, $C = G_D \geq 0$ and the saturation function is defined as $[\cdot]_{\bar{u}^l} = \min[\max[\cdot, 0], \bar{u}^l]$. One possible choice for antialiasing $e_1^l(t)$ is to use periodic-averaging filter, i.e., $e^l[k] = \frac{1}{T_1} \int_{(k-1)T_1}^{kT_1} q(t)dt - q_T^l$. An integrated version of Eq. (4.15) seems infeasible because the following term of the integrated equation

$$-BT_1 \sum_{i=0}^k e_1^l[i]$$

goes to infinity as k goes to infinity for underloaded links where $q^l(\cdot) = 0$.

For the PII^2 model, a recommended implementation for computation of $u^l(t)$ is given by

$$\begin{aligned} u^l[k] = & \left[2u^l[k-1] - u^l[k-2] - \frac{1}{|\hat{Q}^l|} \left(AT_2(e_2^l[k] - e_2^l[k-1]) \right. \right. \\ & \left. \left. + BT_2^2 e_2^l[k] + C(e_2^l[k] - 2e_2^l[k-1] + e_2^l[k-2]) \right) \right]_{\bar{u}^l} \end{aligned} \quad (4.16)$$

where $A = H_I/\bar{\tau} > 0$, $B = H_{I2}/\bar{\tau}^2 \geq 0$ and $C = H_P \geq 0$. One possible choice for antialiasing $e_2^l(t)$ is to use $e_2^l[k] = \frac{1}{T_2}q^{l+}[k] - \alpha_T^l\mu$ where $q^{l+}[k]$ is the byte sum of packets enqueued during the time interval $((k-1)T_2, kT_2]$.

4.6.3 Rate-Based Pricing Scheme

The main advantage of our utility max-min architecture is that the objective of flow control is achieved in a *distributed* manner. However, this advantage might be a drawback in view of fairness because a selfish user can choose a utility function that assigns him a larger data rate. For example, an elastic flow can intentionally disguise itself as a premium flow to attain a larger bandwidth share. Let us consider a simple pricing scheme that charges users by the actual size of data they send into the network. That is to say, user i will be charged $p_i = b_i c$, where b_i is the total bytes transmitted by user i (or flow i) and c is the cost of transmitting unit byte in the network. One crucial problem with this pricing scheme is that there is no penalty for disguised users because they are charged based on the byte-usage of their applications in the network. An FTP user will try to transmit a fixed-size file in a short time by choosing a premium utility because there is no penalty when they send data at a higher rate by choosing more slowly increasing utility functions.

One way to prevent this kind of selfish actions while achieving *genuine* utility max-min fairness is to introduce weights $w(\bar{a}_i)$ where \bar{a}_i is the average data rate of user i during flow's duration and $w(\bar{a}_i)$ is an increasing function of \bar{a}_i . Then, user i will be charged $p_i = w(\bar{a}_i) \cdot b_i c$. If an elastic flow disguises itself as a premium flow to transmit a fixed-size file, it is charged higher for transmitting the file because the premium utility function will assign him a higher data rate and $w(\bar{a}_i)$ will be larger. Real-time and stepwise flows willingly pay more than elastic flows because they need more bandwidth to reach the comparable application-performance levels. In the existing flow control algorithms that support only "best-effort flows", there has been no way to guarantee users' various application-specific performance levels. In utility max-min architecture, network operators now can get more revenue since the satisfied users now have willingness to pay more for apparently visible performance gain. Note that the network still does not need to know users' utility functions in our proposed pricing scheme. Including our proposed pricing scheme, there might be various pricing schemes to prevent users from cheating.

Table 4.1: Parameters Used for Simulation.

q_T^l	T_1	α_T^l	T_2	δ	λ	DPS	W
$0.05\bar{\tau}\mu^l$	30Δ	0.95	100Δ	0.9	0.98	500bytes	300Δ

4.7 Simulation Results

Using the four types of utility given in Section 4.5, we provide a number of simulation results using ns-2 simulator [32] to demonstrate the merits of utility max-min flow control and the performance of our algorithms. In both scenarios, the largest round-trip propagation delays are set to 100ms. To take queueing delays and sampling delays at links into consideration, $\bar{\tau}$ is set to a slightly greater value than this. Other parameters used for simulation is given in Table 4.1 where Δ is one data packet transmission time, i.e., $\Delta \triangleq \text{DPS}/\mu^l$. To avoid messy figures, we simulated our architecture with only two kinds of three-term link controllers, i.e., PID and PII^2 controllers. Simulation results for the PID and PII^2 link controller models are respectively denoted by G_{PID}^3 and $G_{PII^2}^3$. For two-term link controllers, i.e., PI and II^2 controllers, we can obtain simulation results similar to those given in Section 3.6.

4.7.1 Scenario 1: Simple Network With Heterogeneous Round-Trip Delays

The network configuration used for Scenario 1 is shown in Fig. 4.8. In this scenario, $\bar{\tau} = 110\text{ms}$ is used. The flow models used in this scenario are summarized in Table 4.2, where each utility corresponds to the utility given in Fig. 4.7. We can see from Table 4.2 that flows experience heterogeneous round-trip delays and the maximum round-trip propagation delay is 100ms. In Fig. 4.9, the queue length at link 1, source utilities and source sending rates are shown. We can see that our proposed algorithms equalize utility values of sources, while the feasibility condition in Definition 4.1 and utility max-min property in Definition 4.2 are satisfied. For the PID model, the link capacity is fully utilized, while the target queue length ($q_T^l = 68.8\text{kbytes}$) is obtained. For PII^2 model, the target utilization ($\alpha_T^l = 0.95$) is achieved, while the queue length at steady state becomes zero. The inverses of utilities, i.e., sending rates, are also shown in Fig. 4.9. It should be noted that the PII^2 model achieves zero queue length at steady states and converges faster than the PID model when some flows

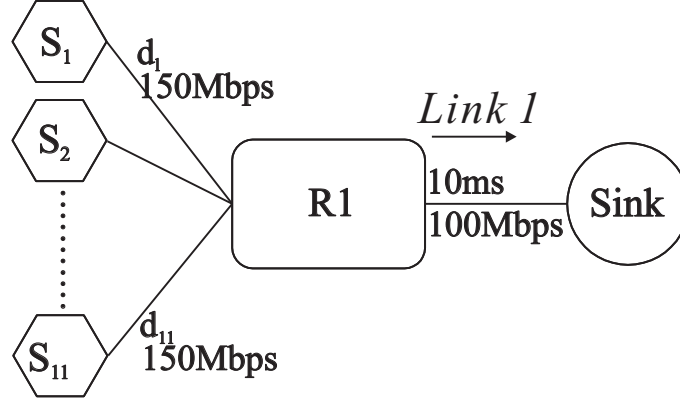


Figure 4.8: Simple network used for Scenario 1

Table 4.2: Flow Models Used for Scenario 1.

source	utility	d_i	begin(s) at	end(s) at
S_1	premium	5ms	$-\infty$	∞
S_2	premium	15ms	$-\infty$	25s
S_3	premium	20ms	$-\infty$	40s
S_4, S_5, S_6	elastic	5, 25, 30ms	5, 5.1, 5.2s	40.1, 40.2, 40.3s
S_7, S_8, S_9	real-time	10, 35, 40ms	10, 10.1, 10.2s	40.4 40.5 40.6s
S_{10}, S_{11}	stepwise	35, 15ms	15, 15.1s	∞

stop their transmission at the cost of 5% underutilization. As discussed in Section 3.2.2, the PII^2 model quickly achieves fair rates because the saturation nonlinearity at empty buffers is eliminated.

Three real-time flows ($S_7 \sim S_9$) achieve data rates slightly greater than the encoding rate (4Mbps) and elastic flows ($S_4 \sim S_6$) achieve smaller data rates. Before $t=40$ s, two stepwise flows, S_{10} and S_{11} achieves data rates slightly greater than the base-layer rate (4Mbps) due to network congestion. As many flows stop transmission at $t=40$ s, they achieve data rates (≥ 12 Mbps) including the enhancement-layer rate (8Mbps). One crucial merit of utility max-min flow control is that multimedia flows are guaranteed minimum data rates except when the network is severely congested. Furthermore, for flows with stepwise utility, additional layers can be assigned when the network is lightly congested.

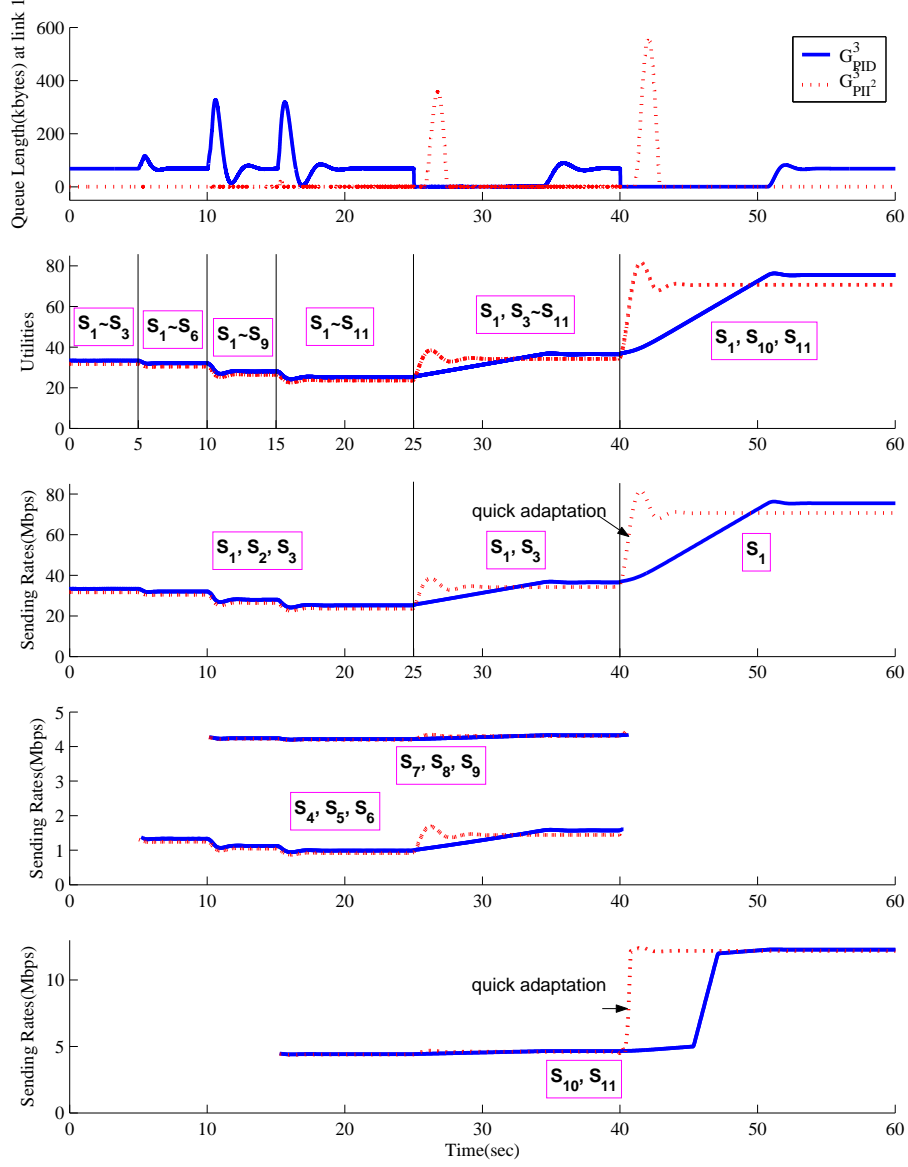


Figure 4.9: Results of Scenario 1 - Queue length at link 1 ($q^1(t)$), Source utilities ($u_i(t)$) and Source sending rates ($a_i(t)$).

Because premium flows have identical utility functions, $U_i(a) = a$, sending rates of premium flows ($a_1(t) \sim a_3(t)$) are nearly identical to source utilities ($u_1(t) \sim u_{11}(t)$) if

we ignore the slight time shift due to feedback delay. For PID model, we provide a revised source algorithm in Appendix 6.8 which suppresses queue length overshoots.

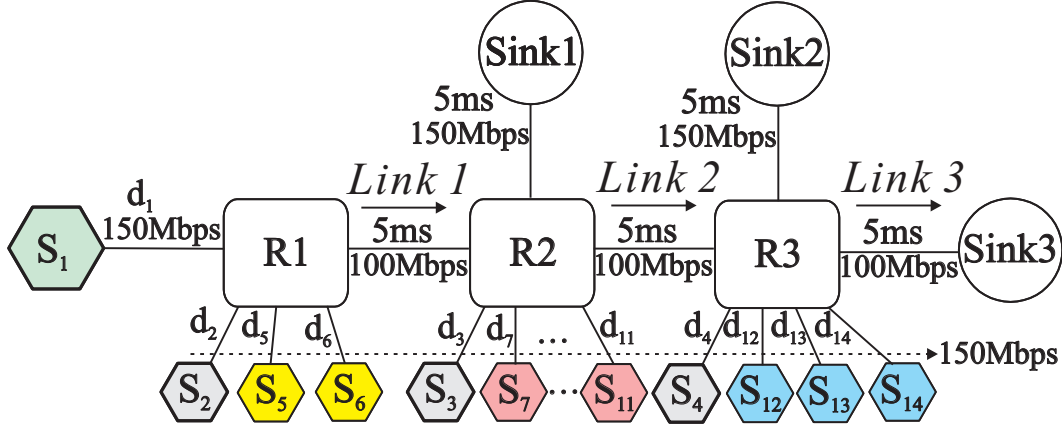


Figure 4.10: Multiple bottleneck network used for Scenario 2

Table 4.3: Flow Models Used for Scenario 2.

source	utility	d_i	begin(s) at	end(s) at	sink
S_1	premium	35ms	$-\infty$	∞	Sink3
S_2	elastic	15ms	$-\infty$	∞	Sink1
S_3	elastic	20ms	$-\infty$	∞	Sink2
S_4	elastic	5ms	$-\infty$	∞	Sink3
$S_5 \sim S_6$	elastic	25, 30ms	10, 10.1s	∞	Sink1
$S_7 \sim S_{11}$	real-time	20, 40, 15, 40, 25ms	20, 20.1, 20.2, 20.3, 20.4s	∞	Sink2
$S_{12} \sim S_{14}$	stepwise	30, 40, 10ms	40, 40.1s	∞	Sink3

4.7.2 Scenario 2: Multiple Bottleneck Network With Heterogeneous Round-Trip Delays

To show that the proposed models work well in multiple bottleneck networks, we consider a network configuration in which there are three bottleneck links; see Fig. 4.10. In this scenario, $\bar{\tau} = 120\text{ms}$ is used. The flow models used in this scenario is summarized in Table 4.3. In Fig. 4.11, although there are queue overshoots at $t=10\text{s}$, 20s , 40s because several flows begin transmission simultaneously, such dramatic events (e.g., $S_7 \sim S_{11}$ begin transmission simultaneously.) do not occur frequently in real networks. In steady states, the sending rates of flows satisfy the feasibility condition and utility max-min property, as

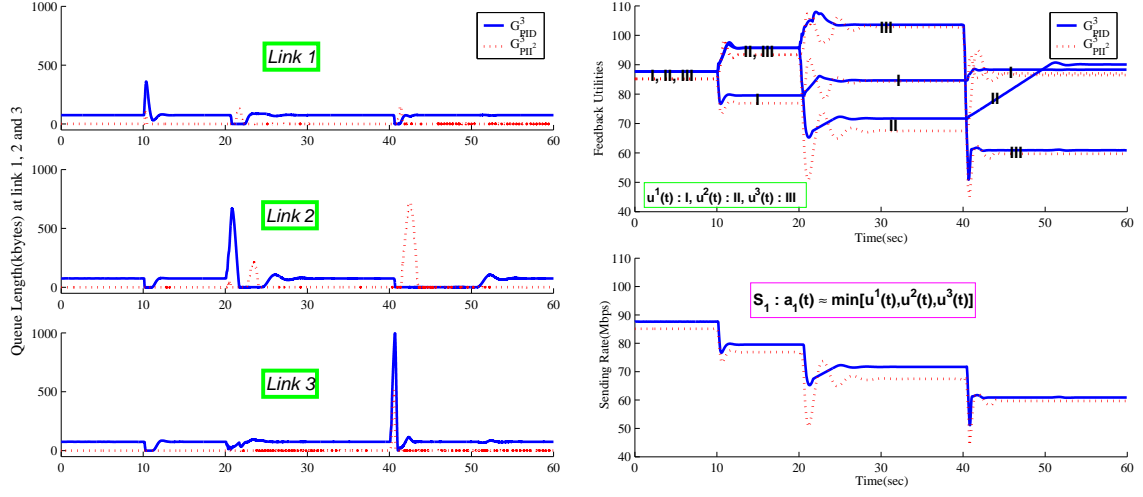


Figure 4.11: Results of Scenario 2 - Queue length at links ($q^l(t)$), Feedback utilities at links ($u^l(t)$) and Source sending rate of S_1 ($a_1(t)$).

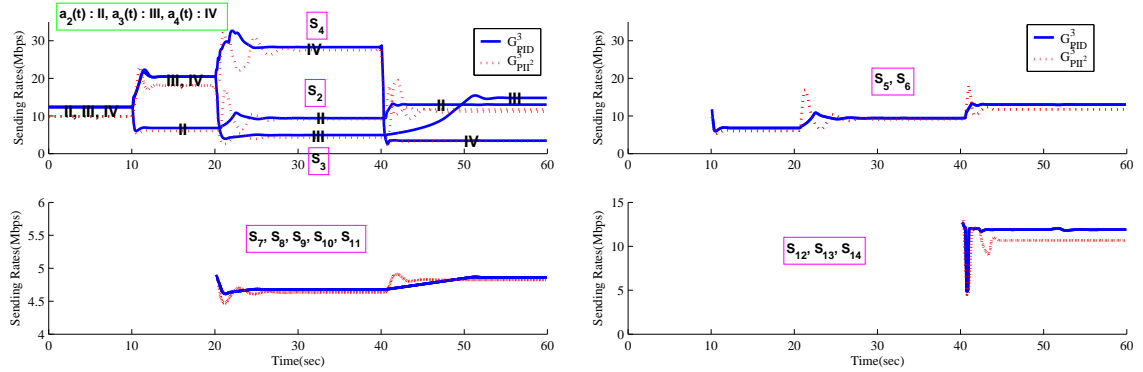


Figure 4.12: Results of Scenario 2 - Source sending rates of $S_2 \sim S_{14}$ ($a_2(t) \sim a_{14}(t)$).

shown in Fig. 4.12. Because S_1 traverses link 1, link 2 and link 3, $a_1(t)$ will be nearly identical to the minimum of the feedback utilities at the three links, $\min[u^1(t), u^2(t), u^3(t)]$. To avoid lengthy presentation, in Scenario 2, we show only the sending rate of premium flow S_1 and feedback utilities at links, instead of the source utilities of flows.

Four intervals are readily distinguishable; $[-\infty, 10s]$, $[10s, 20s]$, $[20s, 40s]$ and $[40s, \infty]$. From $-\infty$ to $t=10s$, S_1 is bottlenecked at all three links. As new elastic flows, S_5 and S_6 destined for Sink1 begin transmission at $t=10s$, S_1 becomes bottlenecked only at link 1.

Thus from $t=10s$ to $t=20s$, flow S_3 and S_4 can send data at higher rates and S_2 can send data at a lower rate compared with the previous time interval, as shown in Fig. 4.12. As five real-time flows, $S_7 \sim S_{11}$ destined for Sink2 begin transmission at $t=20s$, S_1 is now bottlenecked at link 2. From $t=20s$ to $t=40s$, S_2 , S_5 and S_6 can send data at higher rates and S_3 can send data at a lower rate compared with the previous time interval. Similarly, when three stepwise flows destined for Sink3 begin transmission at $t=40s$, S_1 becomes bottlenecked at link 3 and flows are allocated bandwidth according to utility max-min fairness. Thus we can verify that our proposed algorithms work well in multiple bottleneck networks where the bottleneck link of a flow can change dynamically as the network situation changes.

CHAPTER 5

CONCLUSION

In Chapter 3, we have provided two network models which satisfy *weighted max-min fairness* and dispense with any kind of per-flow operation in routers. We have found equivalent stability conditions in two network models with heterogeneous round-trip delays. The theorem states that a stabilizing gain found with homogeneous-delay τ also stabilizes all the networks with heterogeneous delays less than or equal to τ and overestimation of the sum of flows' weights is completely safe. We derive the equivalent condition for the asymptotic stability of the network as an explicit and usable function of the upper bound $\bar{\tau}$ of all round-trip delays. We show that the gain sets maximizing the asymptotic decay rates do not cause the serious performance degradation even though they are obtained using only an upper bound of round-trip delays.

The PID model achieves not only full utilization but also the target queue length at its equilibrium point. The PII² model achieves zero queueing delays and absorbs transient overshoots in links sacrificing some degree of utilization, and α_T^l can be lowered to absorb the transient queues when many short-live flows exist. It also rapidly achieves fair rates because the saturation nonlinearity at empty buffers is now eliminated. We believe that our analytical and experimental results will play an important role in encouraging the usage of more sophisticated flow control algorithms in packet networks.

In Chapter 4, we have proposed a control-theoretic framework for application-performance oriented flow control. Our contribution is three-fold. First, we have found a distributed link algorithm that attains utility max-min bandwidth sharing while controlling link buffer occupancy to either zero or a target value. Moreover, the link algorithm does not require any per-flow information and processing, so it is scalable. Second, our algorithm is shown to

be asymptotically stable in the presence of round-trip delays for arbitrary forms of utility function, as long as they are continuous and their slopes are larger than a certain positive constant. Third, our framework lends itself to a single unified flow control scheme that can simultaneously serve, not only elastic flows, but also non-elastic flows such as voice, video and layered video.

Although the stability results given in the first part of this dissertation have been derived for a single bottleneck network with heterogeneous round-trip delays, and those given in the second part have been derived for a single bottleneck network with homogeneous round-trip delays, we were able to see through simulations that the proposed algorithm in the first part works well for a multiple bottleneck network and the proposed algorithm in the second part works well for a multiple bottleneck network with heterogeneous round-trip delays. In future work, we will extend the stability results to that general case.

In our network models, sources induce overshoots of queue lengths because they immediately adapt to the network-assigned data rates. Although our models, especially the three-term controller in the PII^2 models, are good at reducing transient queues when there are many flows, one may change the source algorithm so that sources adapt to allocated data rates smoothly and, as a result, the queue length overshoots are suppressed when there are small number of flows or when the portion of short-lived flows is large. To achieve fair rates in a short time while reducing queue length overshoots, we present one revised source algorithm for PID link controller model in Appendix 6.8. We suggest that one may use several techniques proposed in XCP [6] to extend our algorithms for TCP-like sources.

CHAPTER 6

APPENDIX

6.1 Proof of Proposition 3.1

Because $G(j\omega) = -j\infty - \infty^2$ in the third quadrant, there always exists a value $\tilde{\omega}$ (shown as the point P_1 in Fig. 6.1) in $0 < \tilde{\omega} < \infty$ such that $\text{Re}[G(j\omega)] < 0$ for all $0 < \omega \leq \tilde{\omega}$. To prove the Proposition, it is sufficient to show that $\text{Im}[G(j\omega)] < 0$ for all $\tilde{\omega} < \omega < \bar{\omega}$. By contradiction, assume that there is a value $\hat{\omega}$ (shown as the point P_2 in Fig. 6.1) in $\tilde{\omega} < \hat{\omega} < \bar{\omega}$ such that $\text{Im}[G(j\hat{\omega})] = 0$. Moreover, from $\text{Im}[G(j\hat{\omega})] = 0$, it follows that $\angle G(j\hat{\omega}) = 0$ or $\angle G(j\hat{\omega}) = \pi$. Since one of two conditions, i.e., $G(j\hat{\omega}) > 1$ or $G(j\hat{\omega}) < -1$ should be satisfied, let us assume the former case. But, $\angle G(j\hat{\omega})$ can not be zero because $-\pi < \angle G_0(j\hat{\omega}) < 0$ and $-\pi < -\bar{\omega}\tau < -\hat{\omega}\tau < 0$. Therefore, this case cannot happen.

Let us assume the latter case, $G(j\hat{\omega}) < -1$. We can summarize the angle values of $G(j\omega)$ as follows.

$$\left\{ \begin{array}{l} \angle G(j0^+) = -\pi \\ -\pi < \angle G(j\tilde{\omega}) < -\frac{\pi}{2} \\ \angle G(j\hat{\omega}) = -\pi \\ -\pi < \angle G(j\bar{\omega}) < 0 \\ \lim_{n \rightarrow \infty} \angle G(j\frac{(2n+1)\pi}{\tau}) = -\pi \end{array} \right.$$

Since the angle function of $G(j\omega)$ is continuous, there should be at least three local extrema.

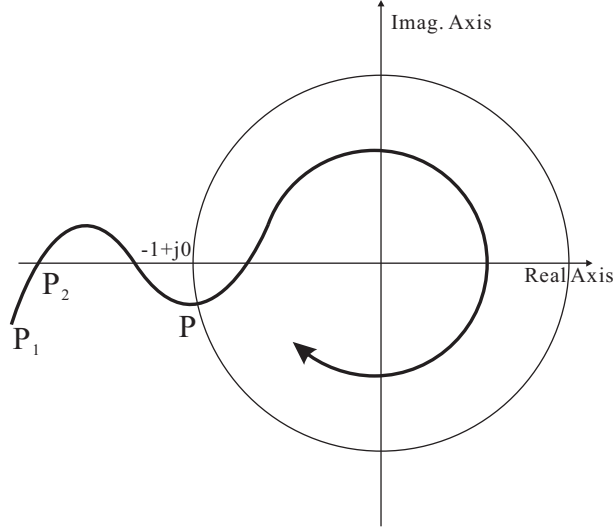


Figure 6.1: Nyquist plot used for Proposition 3.1.

The angle function and its derivative which can be obtained from Eq. (3.12) are given by

$$\begin{cases} \psi(\omega) \equiv \angle G(j\omega) = \arctan\left(\frac{g_D\omega^2 - g_I}{g_P\omega}\right) - \frac{\pi}{2} - \omega\tau \\ \psi'(\omega) = \frac{g_P g_D \omega^2 + g_P g_I}{g_P^2 \omega^2 + (g_D \omega^2 - g_I)^2} - \tau. \end{cases}$$

Because $\psi'(\omega) = 0$ is a biquadratic equation, there are at most two solutions in $0 < \omega < \infty$. This is in contradiction with the fact that $\psi(\omega)$ has at least three local extrema.

6.2 Proof of Theorem 3.1

Sufficiency. We can see easily from Fig. 3.2 that the Nyquist plot has a unique intersection with the unit circle in $0 < \omega < \infty$. More formally, there is a unique positive solution to the following equation if $|g_D| < 1$, $R \geq 1$ and $g_I > 0$ (The case $g_I = 0$ also can be treated in a similar way.),

$$|G(j\omega)| = |G_0(j\omega)| = \left(g_D - \frac{g_I}{\omega^2}\right)^2 + \left(\frac{g_P}{\omega}\right)^2 = R^2, \quad (6.1)$$

because Eq. (6.1) is equivalent to the following biquadratic equation

$$(R^2 - g_D^2)\omega^4 + (2g_D g_I - g_P^2)\omega^2 - g_I^2 = 0, \quad (6.2)$$

and the condition for Eq. (6.2) to have a unique positive solution is equivalent to

$$(2g_D g_I - g_P^2)^2 + 4g_I^2(R^2 - g_D^2) \geq 0$$

$$\text{and} \quad -g_I^2(R^2 - g_D^2) < 0,$$

which is already satisfied by the assumption of g_D and R . This means that the Nyquist plot reaches the unit circle and never depart from it. That is, the part of the Nyquist plot corresponding to $\omega > \bar{\omega}$ is entirely contained in the unit circle so that it can never contribute to encircling or touching $-1 + j0$. If the assumption of τ is satisfied, we can easily see that the Nyquist plot of $G(j\bar{\omega})$ is always below $-1 + j0$ for $0 < \omega \leq \bar{\omega}$ and all the assumptions of Proposition 3.1 are satisfied. Therefore, the Nyquist plot neither does encircle nor touch $-1 + j0$ because $\text{Im}[G(j\omega)] < 0$ for all ω in $0 < \omega \leq \bar{\omega}$. The open-loop pole $s = 0$ can be managed with the boundary deviation technique by adding an infinitesimal half-circle. Appealing to the Nyquist stability criterion, we have proven the stability of closed-loop system.

Necessity can be proven trivially. If $|g_D| \geq 1$ or the condition of Eq. (3.14) is violated, the Nyquist plot simply encircles or touches $-1 + j0$.

6.3 Proof of Corollary 3.1

Here we give a sketch of proof because a detailed proof requires complicated arguments. To find a necessary condition, let us assume that $0 < G_D < 1$ is fixed. From the fact that $\arccos(\cdot)$ is a monotonically decreasing function, we see that $G_I < \omega_1^2 (G_D + \cos(\omega_1))$ and $\omega_1 < \arccos(-G_D)$. We can consider two cases, i.e., $0 < \omega_1 \leq \frac{\pi}{2}$ and $\frac{\pi}{2} < \omega_1 < \arccos(-G_D)$. Considering carefully both two cases and using the fact that the function $\omega \sin(\omega)$ has a unique maximum over the interval $0 < \omega < \pi$, it follows that

$$G_P < \begin{cases} \omega_1 \sin(\omega_1) & \text{over } \frac{\pi}{2} < \omega_1 < \arccos(-G_D) \\ \text{if } \arccos(-G_D) < \omega_0, \\ \omega_0 \sin(\omega_0) & \text{if } \omega_0 \leq \arccos(-G_D), \end{cases} \quad (6.3)$$

This equation can be used in obtaining a necessary stability condition for G_P which is given by Eq. (3.18). The case $G_D = 0$ can be easily treated separately and can be found by setting $G_D = 0$ in Eq. (3.18).

Let us assume that $0 \leq G_D < 1$ is fixed and $G_P > 0$ takes a fixed value such that $G_P = \omega_* \sin(\omega_*)$ and $0 < \omega_* < \arccos(-G_D)$ which is the same to the range of ω_1 . When $\arccos(-G_D) < \omega_0$, G_I is simply given by $G_I < \omega_*^2(G_D + \cos(\omega_*))$ from Eq. (3.15). When $\omega_0 \leq \arccos(-G_D)$, we have to consider two cases, i.e., $0 < \omega_* < \omega_0$ and $\omega_0 \leq \omega_* < \arccos(-G_D)$, separately. Considering in this way, it can be shown that a necessary stability condition for G_I is given by Eq. (3.19).

Although we omit the proof of sufficiency, it can be verified with direct substitution of Eqs. (3.17), (3.18) and (3.19) into Eqs. (3.15) and (3.16).

6.4 Proof of Theorem 3.2

Proof of necessity is trivial. If the heterogeneous-delay case is asymptotically stable, then we can simply set $\rho_1 = 1$, $\rho_i = 0$, $\forall i \geq 2$ and $\tau_1 = \bar{\tau}$.

For the proof of sufficiency, both conditions of Proposition 3.2 should be satisfied. We immediately see that the first condition of Proposition 3.2 is already satisfied because we have a choice of $2|Q|$ -tuple vector, i.e., $\rho_1 = 1$, $\rho_i = 0$, $\forall i \geq 2$ and $\tau_1 = \bar{\tau}$ which stabilizes the homogeneous-delay case. For the second condition, let us define a circular sector as follows:

$$S_\omega^{\bar{\tau}} = \{s \in \mathcal{C} \mid |s| \leq 1, \text{ and } -\bar{\tau}\omega \leq \angle s \leq 0\}.$$

Let us define z as $z \equiv \sum_{i \in Q} \rho_i \exp(-j\tau_i \omega)$. By rewriting z in terms of $\exp(-j\tau_i \omega)$ and 0 as follows:

$$z = \sum_{i \in Q} \rho_i \exp(-j\tau_i \omega) + \left(1 - \sum_{i \in Q} \rho_i\right) \cdot 0,$$

we see that $z \in S_\omega^{\bar{\tau}}$ because $S_\omega^{\bar{\tau}}$ is a convex set and z is a convex combination of $|Q| + 1$ points in $S_\omega^{\bar{\tau}}$. Furthermore, if we define a set $G_0(j\omega)S_\omega^{\bar{\tau}} \equiv \{G_0(j\omega) \cdot s \mid s \in S_\omega^{\bar{\tau}}\}$ which is depicted in Fig. 6.2, we see that $V(\omega) \subset G_0(j\omega)S_\omega^{\bar{\tau}}$ for all ω because the following equation holds:

$$G(j\omega, \boldsymbol{\rho}, \boldsymbol{\tau}) = G_0(j\omega)z(j\omega, \boldsymbol{\rho}, \boldsymbol{\tau}) \in G_0(j\omega)S_\omega^{\bar{\tau}}.$$

Since the circular sector $G_0(j\omega)S_\omega^{\bar{\tau}}$ is bounded by two functions, i.e., $G_0(j\omega)\exp(-j\bar{\tau}\omega)$ and $G_0(j\omega)$ and the magnitudes of two functions are equal to $|G_0(j\omega)| = |G(j\omega)|$, the

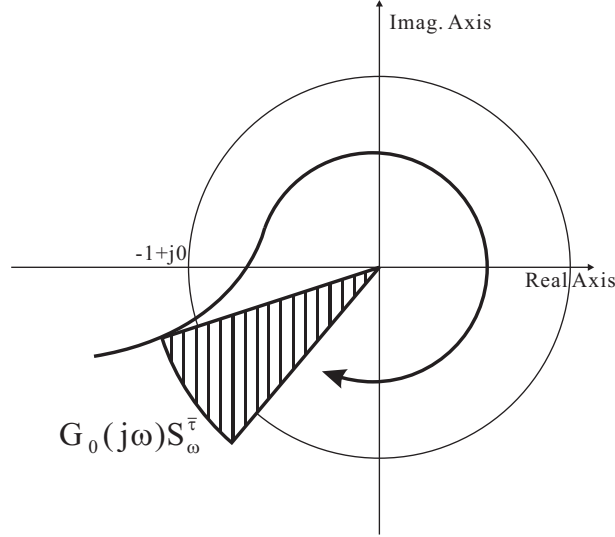


Figure 6.2: Nyquist plot used for Theorem 3.2.

circular sector $G_0(j\omega)S_{\omega}^{\bar{\tau}}$ can be expressed as follows:

$$G_0(j\omega)S_{\omega}^{\bar{\tau}} = \{z \mid \eta_l \leq \angle z \leq \eta_u, |z| \leq |G_0(j\omega)|\}, \quad (6.4)$$

$$\eta_l \equiv \angle G_0(j\omega) \exp(-j\bar{\tau}\omega) = \angle G_0(j\omega) - \bar{\tau}\omega, \quad \eta_u \equiv \angle G_0(j\omega).$$

For $\bar{\omega} < \omega$, where $|z| < 1$ for all $z \in G_0(j\omega)S_{\omega}^{\bar{\tau}}$, the sector $G_0(j\omega)S_{\omega}^{\bar{\tau}}$ is completely contained inside the unit circle. Naturally, $V(\omega)$, which is a subset of $G_0(j\omega)S_{\omega}^{\bar{\tau}}$ does not touch $-1 + j0$. For $0 < \omega \leq \bar{\omega}$, $\text{Im}[G_0(j\omega)] < 0$ and $\text{Im}[G_0(j\omega)\exp(-j\bar{\tau}\omega)] < 0$ hold by Proposition 3.1. Thus, $-\pi < \eta_l < 0$ and $-\pi < \eta_u < 0$ hold. From Eq. (6.4), we see that $G_0(j\omega)S_{\omega}^{\bar{\tau}}$ is completely contained in the lower half plane. For $\omega = 0$, the value set $V(\omega)$ is infinity. By Proposition 3.2, we now complete the proof of sufficiency.

6.5 Proof of Theorem 4.1

If all links in the network perform the same operation as that described in Section 4.3, each flow has its own bottleneck link (which can be more than one) and the utility vector at steady state is feasible in the sense that it satisfies Eq. (4.10) for all bottleneck links $l \in L$. If we increase the utility value of flow i which is bottlenecked at some link l while maintaining feasibility, we should reduce the data rate of flow $i' (\neq i)$ that traverses link

l , i.e., $i' \in N(l)$. Since $U_{i'}(\cdot)$ is an increasing function by the assumption A.1, the utility value of i' is also reduced. Since $U_{i'}(a_{i's}) \leq U_i(a_{is})$ for all $i' \in N(l)$ by the definition of bottleneck link (See, e.g., [1].), we are reducing the utility value of flow i' , which is already less than or equal to the utility value of flow i . By Definition 4.2, we complete the proof. To the PII² model, a similar proof is applicable.

6.6 Proof of Theorem 4.2

For notational simplicity, we define two functions shown in Fig. 4.5 as follows.

$$\bar{G}(s) \triangleq G(s)/(1 + hG(s)), \quad \bar{\mathcal{U}}^{-1}(u) \triangleq \mathcal{U}^{-1}(u) - hu.$$

By the assumption that (G_D, G_P, G_I) is contained in Fig. 3.3, we can see that $\bar{G}(s)$ is asymptotically stable for any $h \in (0, 1]$ from the arguments of Section 3.3.3. Then we can apply the Dewey and Jury's criterion (Corollary 5 in [37]) to our nonlinear monotone feedback system because $\bar{G}(s)$ is asymptotically stable so that $g(t)$ and $\dot{g}(t)$ become elements of $L_1(0, \infty)$, i.e., the set of absolutely integrable functions and $\bar{\mathcal{U}}^{-1}(0) = 0$ by the assumption A.2. Although the differentiability of feedback nonlinearities was also assumed, this assumption is used only for the simplicity of their proof. If the feedback nonlinearities have left-hand and right-hand derivatives at all points, Dewey and Jury's criterion still holds.

If there exist a finite number η and a finite number $\kappa \geq 0$ such that the inequality (4.12) is satisfied for some small $h > 0$, then the closed-loop system is asymptotically stable with $\mathcal{U}^{-1}(u)$ satisfying the following equation by Dewey and Jury's criterion.

$$0 \leq \frac{d}{du} (\mathcal{U}^{-1}(u) - hu) \leq \frac{1}{k}.$$

If this is satisfied for arbitrarily small $h > 0$, we have the following condition for $\mathcal{U}^{-1}(u)$.

$$0 < \frac{d\mathcal{U}^{-1}(u)}{du} \leq \frac{1}{k}. \quad (6.5)$$

When each of the utility functions, $U_i(a)$, satisfies $k \leq dU_i/da < \infty$, then it also satisfies $0 < d\mathcal{U}_i^{-1}/du \leq 1/k$ and their sum becomes as follows, due to the finitude of $|Q|$.

$$0 < \frac{1}{|Q|} \sum_{i \in Q} \frac{d\mathcal{U}_i^{-1}(u)}{du} \leq \frac{1}{k} \iff 0 < \frac{d\mathcal{U}^{-1}(u)}{du} \leq \frac{1}{k}.$$

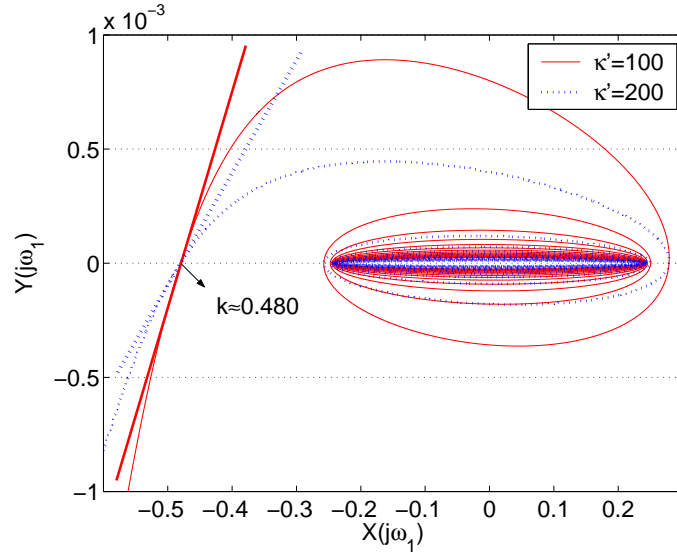
Therefore, we can conclude that the closed-loop system is asymptotically stable if the minimum slope of the utility functions is restricted by k , i.e., $k \leq dU_i/da < \infty \forall, a \in [0, \infty)$. For the PII^2 model, we can apply the same procedure because $G(s)$ of the PII^2 model is identical to that of the PID model.

6.7 Proof of Corollary 4.1

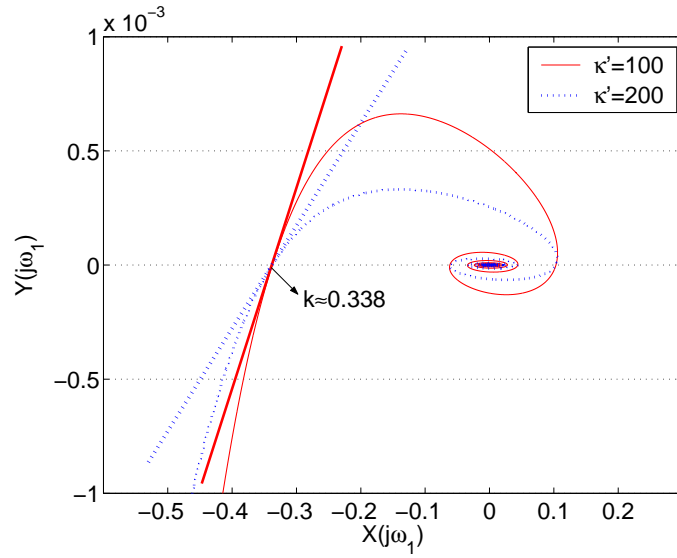
To apply Theorem 4.2, the condition of Eq. (4.13) should be satisfied for h arbitrarily close to 0. When we use a graphical technique with small h , κ' has an essential role in achieving a smaller k . Eq. (4.13) implies that κ' has no significant effect when ω_1 is small and in that case the $(X(\omega_1), Y(\omega_1))$ trajectories are nearly identical, independent of κ' . However, when ω_1 is sufficiently large and κ' is very small, $Y(\omega_1)$ becomes very large and the trajectories of $(X(\omega_1), Y(\omega_1))$ prevents us from obtaining a smaller k value. To visualize, a sample trajectory when G_{PID}^3 is used with $h = 0.001$ and $\kappa' = 0$ is shown in Fig. 4.6. In this figure, the value of k must be at least 2500. Thus, we have to use κ' to find a smaller k value. Using the graphical technique shown in Fig. 6.3, we can show that the following k values satisfy $X(\omega_1) - \eta'Y(\omega_1) + k > 0, \forall \omega_1 \geq 0$ for some $\eta' \triangleq \eta/\tau$ and $\kappa' \geq 0$.

$$k = \frac{G_P}{\omega_1^* \sin \omega_1^*} + \epsilon$$

where ω_1^* is the smallest $\omega_1 > 0$ satisfying $\frac{G_I - \omega_1^2 G_D}{\omega_1^2} \sin(\omega_1) - \frac{G_P}{\omega_1} \cos(\omega_1) = 0$ and $\epsilon > 0$ is any finite number. For G_{PID}^3 and G_{PID}^2 , values of $\frac{G_P}{\omega_1^* \sin \omega_1^*}$ are approximately 0.4798 and 0.3375, respectively. Thus we complete the proof.



(a) For G_{PID}^3 with $h = 0.001$ and $\kappa' = 100, 200$.



(b) For G_{PID}^2 with $h = 0.001$ and $\kappa' = 100, 200$.

Figure 6.3: Two samples of $(X(\omega_1), Y(\omega_1))$ plot for G_{PID}^3 and G_{PID}^2 .

6.8 Source Algorithm Revision

The source algorithm, given by Eq. (4.4), assumes a source to adjust its sending rate immediately, to the inverse of the minimum utility value. Therefore, a source can adapt to the network assigned utility value very fast. Note that this advantage is obtained at the cost of queue length overshoots in router buffers which can be problematic. For PID link controller model, Figs. 4.9, 4.11 and 4.12 imply that queue length overshoots occur in a link only when a new flow becomes bottlenecked at that link, that is to say, when $|Q^l|$ increases. Let us denote by t_i^0 the time at which flow i receives the first feedback utility value after beginning its transmission. We present one candidate source algorithm in Eq. (SA') by introducing a boolean variable $isInit$ and a constant γ which should be greater than 1.

$$\begin{cases} a_i(t) = \frac{1}{\gamma} U_i^{-1}(u_i(t)) \text{ and } isInit = 1, & \text{if } t = t_i^0 \\ \dot{a}_i(t) = \frac{1}{\gamma\tau} U_i^{-1}(u_i(t)) & , \text{ if } t > t_i^0 \text{ and } a_i(t) < U_i^{-1}(u_i(t)) \text{ and } isInit == 1 \\ a_i(t) = U_i^{-1}(u_i(t)) \text{ and } isInit = 0 & , \text{ if } t > t_i^0 \text{ and } a_i(t) \geq U_i^{-1}(u_i(t)) \text{ and } isInit == 1 \\ a_i(t) = U_i^{-1}(u_i(t)) & , \text{ otherwise} \end{cases} \quad (SA')$$

When $isInit$ is 1, the flow is in initial phase otherwise the flow is in normal phase and accords with Eq. (3.2). With this revised source algorithm, a source increases its sending rate from $\frac{1}{\gamma} U_i^{-1}(u_i(t))$ to the inverse of the minimum utility value linearly in initial phase. Thus we can expect that γ can regulate the speed of rate adaptation effectively.

We also implemented an approximate version of this source algorithm in ns-2 simulator. Simulation results for PID controller model using the same flow models and network configuration of Scenario 1 are shown in Fig. 6.4. We can see that sending rates of flows increase carefully during initial phases. The choice of γ presents us several tradeoffs. While a larger γ results in a faster convergence speed, a smaller γ allows faster rate adaptation of flows. To quantify queue length behavior of source algorithms, we define three performance indices as follows.

$$qmax^l \triangleq \max_t [q^l(t)], \quad qov^l \triangleq \max_t [q^l(t) - q_T^l],$$

$$[\text{percent overshoot}]^l \triangleq \frac{qov^l}{q_T^l} \times 100\%.$$

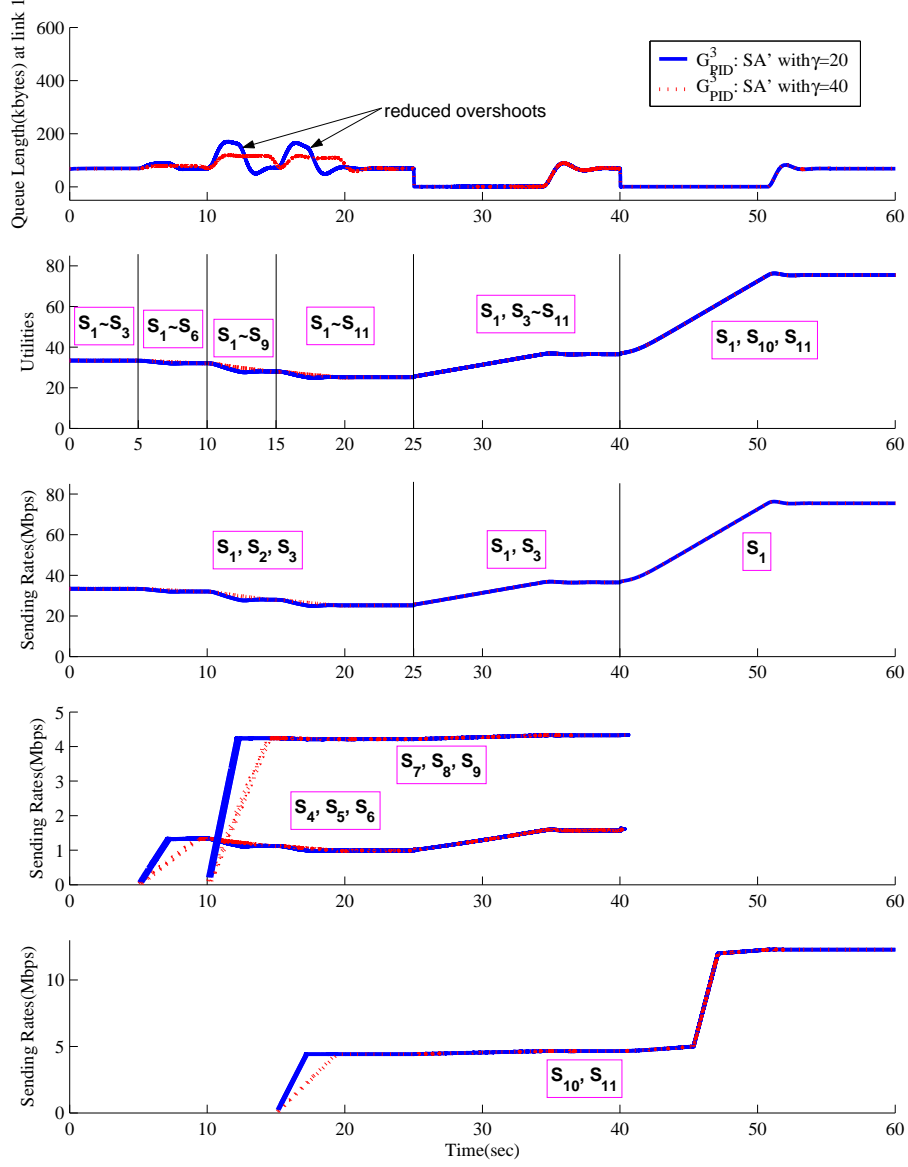


Figure 6.4: Results of Scenario 1 with the revised source algorithm - Queue length at link 1 ($q^1(t)$), Source utilities ($u_i(t)$) and Source sending rates ($a_i(t)$).

Table 6.1, where $q_T^1 = 68.8\text{kbytes}$, shows that the queue length overshoot and the percent overshoot become smaller as γ becomes larger. Compared with AIMD (additive increase

Table 6.1: Queue Length Overshoots of Scenario 1 for SA and SA'. ($q_T^1 = 68.8\text{kbytes}$)

source algorithm	link algorithm	q_{max}^1	q_{ov}^1	[percent overshoot] ¹
SA (Fig. 4.9)	PID	328.5kbytes	259.8kbytes	377.8%
SA' with $\gamma = 20$ (Fig. 6.4)	PID	171.0kbytes	102.3kbytes	148.7%
SA' with $\gamma = 40$ (Fig. 6.4)	PID	120.5kbytes	51.8kbytes	75.3%

multiplicative decrease) in TCP congestion control which results in sluggish convergence when the bandwidth-delay product is large, our revised source algorithm achieves fair rates roughly within $\gamma\bar{\tau}$ seconds irrespective of the bandwidth-delay product.

References

- [1] D. Bertsekas and R. Gallager, *Data Networks*. New Jersey: Prentice Hall, 1992.
- [2] F. Kelley, “Charging and rate control for elastic traffic,” *Euro. Trans. Telecommun.*, vol. 8, pp. 33–37, 1997.
- [3] L. Massoulié and J. Roberts, “Bandwidth sharing: Objectives and algorithms,” in *Proceedings of IEEE INFOCOM*, 1999, pp. 1395–1403.
- [4] A. Tang, J. Wang, and S. H. Low, “Is fair allocation always inefficient,” in *Proceedings of IEEE INFOCOM*, 2004, pp. 35–45.
- [5] C. Jin, D. X. Wei, and S. H. Low, “FAST TCP: Motivation, architecture, algorithms, performance,” in *Proceedings of IEEE INFOCOM*, 2004, pp. 2490–2501.
- [6] D. Katabi, M. Handley, and C. Rohrs, “Congestion control for high bandwidth-delay product networks,” in *Proceedings of ACM SIGCOMM*, 2002.
- [7] S. Chong, S. H. Lee, and S. H. Kang, “A simple, scalable, and stable explicit rate allocation algorithm for max-min flow control with minimum rate guarantee,” *IEEE/ACM Trans. Networking*, vol. 9, no. 3, pp. 322–335, June 2001.
- [8] P. Ranjan, E. H. Abed, and R. J. La, “Nonlinear instabilities in TCP-RED,” in *Proceedings of IEEE INFOCOM*, 2002, pp. 249–258.
- [9] V. Misra, W.-B. Gong, and D. Towsley, “Fluid-based analysis of a network of AQM routers supporting TCP flows with an application to RED,” in *Proceedings of ACM SIGCOMM*, 2000, pp. 151–160.
- [10] C. V. Hollot, V. Misra, D. Towsley, and W.-B. Gong, “A control theoretic analysis of RED,” in *Proceedings of IEEE INFOCOM*, 2001, pp. 1510–1519.

REFERENCES

- [11] B. Vandalore, S. Fahmy, R. Jain, R. Goyal, and M. Goyal, "General weighted fairness and its support in explicit rate switch algorithms," *Comp. Commun.*, vol. 23, no. 2, pp. 149–161, Jan. 2000.
- [12] F. Kelley, A. Maulloo, and D. Tan, "Rate control for communication networks: shadow prices, proportional fairness and stability," *J. Oper. Res. Soc.*, vol. 49, no. 3, pp. 237–252, Mar. 1998.
- [13] S. Low and D. Lapsley, "Optimization flow control–I: Basic algorithms and convergence," *IEEE/ACM Trans. Networking*, vol. 7, no. 6, pp. 861–875, Aug. 1999.
- [14] R. La and V. Anantharam, "Utility-based rate control in the Internet for elastic traffic," *IEEE/ACM Trans. Networking*, vol. 10, no. 2, pp. 272–286, Apr. 2002.
- [15] J. Mo and J. Walrand, "Fair end-to-end window-based congestion control," *IEEE/ACM Trans. Networking*, vol. 8, no. 5, pp. 556–567, Oct. 2000.
- [16] Z. Cao and E. W. Zegura, "Utility max-min: An application-oriented bandwidth allocation scheme," in *Proceedings of IEEE INFOCOM*, 1999, pp. 793–801.
- [17] P.-F. Quet, B. Ataşlar, A. İftar, H. Özbay, S. Kalyanaraman, and T. Kang, "Rate-based flow controller for communication networks in the presence of uncertain time-varying multiple time-delays," *Automat.*, vol. 38, no. 6, pp. 917–928, June 2002.
- [18] A. Arulambalam, X. Chen, and N. Ansari, "Allocating fair rates for available bit rate service in ATM networks," *IEEE Communications Magazine*, vol. 34, no. 11, pp. 92–100, Nov. 1996.
- [19] S. Kalyanaraman, R. Jain, R. Goyal, S. Fahmny, and B. Vandalore, "The ERICA switch algorithm for ABR traffic management in ATM networks," *IEEE/ACM Trans. Networking*, vol. 8, no. 1, pp. 87–98, Feb. 2000.
- [20] L. Benmohamed and S. Meerkov, "Feedback control of congestion in packet switching networks: The case of single congested node," *IEEE/ACM Trans. Networking*, vol. 1, no. 6, pp. 693–708, Dec. 1993.
- [21] H. K. Khalil, *Nonlinear Systems*. NJ: Upper Saddle River: Prentice Hall, 2002.

REFERENCES

- [22] F. Blanchini, R. L. Cigno, and R. Tempo, "Robust rate control for integrated services packet networks," *IEEE/ACM Trans. Networking*, vol. 10, no. 5, pp. 644–652, Oct. 2002.
- [23] D. Rubenstein, J. Kurose, and D. Towsley, "The impact of multicast layering on network fairness," *IEEE/ACM Trans. Networking*, vol. 10, no. 2, pp. 169–182, Apr. 2002.
- [24] F. Ren, C. Lin, X. Ying, X. Shan, and F. Wang, "A robust active queue management algorithm based on sliding mode variable structure control," in *Proceedings of IEEE INFOCOM*, 2002, pp. 13–20.
- [25] R. C. Dorf and R. H. Bishop, *Modern Control Systems*. Addison-Wesley, 1995.
- [26] J. Ackermann, *Robust Control: Systems with Uncertain Physical Parameters*. New York: Springer-Verlag, 1993.
- [27] L. Benmohamed and S. Meerkov, "Feedback control of congestion in packet switching networks: The case of multiple congested node," *Int. J. Commun. Syst.*, vol. 10, no. 5, pp. 227–246, 1997.
- [28] B. Wyrowski, L. L. H. Andrew, and M. Zukerman, "MaxNet: A congestion control architecture for scalable networks," *IEEE Communications Letters*, vol. 7, no. 10, pp. 511–513, Oct. 2003.
- [29] B. R. Barmish, *New Tools for Robustness of Linear Systems*. New York: MacMillan, 1994.
- [30] J. K. Hale and S. M. V. Lunel, *Introduction to Functional Differential Equations*. London: Springer-Verlag, 1993.
- [31] R. Bellman and K. L. Cooke, *Differential-Difference Equations*. New York: Academic Press, 1963.
- [32] UCB/LBNL/VINT Network Simulator–ns (Version 2.1b9a). [Online]. Available: <http://www.isi.edu/nsnam/ns/>
- [33] B. Radunović and J.-Y. LeBoudec, "A unified framework for max-min and min-max fairness with applications," in *Proc. of Annual Allerton Conference*, 2002.

REFERENCES

- [34] M. Aizerman, “On a problem relating to the global stability of dynamic systems,” *Uspehi Mat. Nauk*, vol. 4, no. 4, 1949.
- [35] M. Vidyasagar, *Nonlinear Systems Analysis*. NJ: Englewood Cliffs: Prentice Hall, 1993.
- [36] R. Kalman, “On physical and mathematical mechanisms of instability in nonlinear automatic control systems,” *J. Appl. Mech. Trans.*, vol. 79, no. 3, pp. 553–566, 1957.
- [37] A. G. Dewey and E. I. Jury, “A stability inequality for a class of nonlinear feedback systems,” *IEEE Trans. Automatic Control*, vol. 11, no. 1, pp. 54–62, Jan. 1966.

요 약 문

통신망에서의 흐름제어에 관한 제어이론적인 접근

본 논문은 최대-최소 대역폭 공평성과 최대-최소 효용 공평성을 달성하는 흐름제어 알고리즘을 제안하며 안정성을 분석하기 위해 제어이론적인 접근 방법을 취하였다. 제안된 알고리즘은 라우터가 개별 흐름의 정보를 저장할 필요가 없으므로 확장성이 있으며, 다양한 지연을 가진 흐름들에 대해 안정함이 증명되어 있으며, 제어기에 사용되는 이득값이 최적으로 조정되어 있다.

먼저, 탄성적 흐름들에 대해 분산적으로 동작하는 최대-최소 대역폭 공평 흐름제어를 위한 망 구조를 제안하며 망 성능을 향상시키기 위해 안정성 조건을 일반화한다. 제안된 흐름제어 알고리즘을 연속 시간 영역에서 표현하는 두 가지의 폐쇄 루프 시스템 모델을 제안하는데, 첫번째 알고리즘은 목표 대기열 길이를 달성하며, 두번째 알고리즘은 목표 활용도를 달성한다. 대기열 길이를 입력 신호로 하여 전송률을 기반으로 동작하는 많은 흐름제어 알고리즘의 수렴이 느린 문제를 두번째 알고리즘으로 해결할 수 있다. 이러한 모델들을 기반으로 하여 왕복 지연이 단일한 경우에 대해 제어 이득값의 조건을 구하고 영점 배제 이론을 적용하여 왕복 지연이 다양한 경우로 조건을 확장한다.

다음으로, 제안된 알고리즘을 개선하여 응용 프로그램의 성능 향상을 목표로 하는 흐름제어 알고리즘을 제안한다. 즉, 탄성적 흐름들과 비탄성적 흐름들을 분산적으로 제어하여 최대-최소 효용 공평성을 달성하는 망 구조를 제안한다. 이 때에 최대-최소 효용 공평성은 대역폭이 아닌 효용값이 최대-최소 공평성을 달성하는 것이다. 또한, 사용자의 효용 함수에 대한 정보를 전혀 사용하지 않는 분산된 링크 알고리즘을 제안한다. 제안하는 알고리즘이 지역적이 아닌 전역적으로 안정화 되는 것을 보여주기 위해서 비선형 제어 이론의 사용이 불가피함을 알 수 있다. 망을 기울기가 제한된 비선형 피드백을 가진 제어 시스템으로 간주하고, 루프 변환 기법과 절대 안정성 이론을 사용하여 망의 안정성을 증명한다. 또한, 분산된 흐름 제어 알고리즘임에도 불구하고, 효용 함수의 최소 기울기가 어떤 양수값보다 크기만 하면 그 어떠한 형태의 효용 함수도 사용될 수 있음을 증명한다. 제안하는 알고리즘은 안정성이 보장되면서

최대-최소 효용 공평성을 분산적으로 달성하는 최초의 알고리즘이다.

제안된 알고리즘들의 실용성과 확장성을 검증하기 위해 다중 병목 망을 포함한 다양한 경우에 대하여 최적 이득값을 이용하여 시뮬레이션한다. 제안된 구조는 탄성적 흐름 뿐만 아니라 음성, 비디오, 다계층 비디오 등의 비탄성적 흐름까지 동시에 지원할 수 있는 통합된 형태의 흐름 제어 알고리즘에 적합하다.

감 사 의 글

박사 학위 논문을 완성하기까지 많은 분들의 도움을 받았습니다. 먼저, 논문의 여러가지 아이디어에 직접적인 도움을 주셨으며, 논문의 전체적인 논지 및 개별적인 문장의 표현을 포함한, 전반적인 연구 내용을 지도해 주신 정송 교수님께 진심으로 감사드립니다. 또한 여러 가지 일로 바쁘신 와중에 논문 심사를 허락해 주시고 새로운 연구방향 등의 건설적인 조언을 주신 성단근 교수님께 감사드리며, 논문의 전반적인 내용에 대하여 여러 가지 구체적인 조언을 주신 이황수 교수님, 바쁘신 와중에 친히 저희 학교까지 오셔서 저의 연구 결과를 다른 교수님께 잘 설명해 주시고 방어해 주신 모정훈 교수님, 그리고 연구분야가 다소 상이함에도 불구하고 논문 내용에 대해 깊이 파악하시고 연구 결과의 한계점까지 지적해 주신 정하웅 교수님께 감사드립니다. 그리고, 학위 논문 계획서를 심사해 주셨던 황강욱 교수님께도 감사드립니다.

긴 시간 동안 같이 지내면서 많은 일들을 함께 기뻐하고 슬퍼했던 네트워크 시스템 연구실의 여러 선후배님들에게, 그 동안 저를 잘 보살펴 주신 것에 대해 깊이 감사드리고 싶습니다. 때로는 시간이 참으로 더디게 느껴지는 순간들도 있었고, 때로는 시간이 참 빠르게 느껴지는 순간들도 있었습니다. 선배들에게는 부담없는 후배가, 후배들에게는 든든한 선배가 되지 못하고, 좀 더 많은 애정을 베풀 수 있었던 시간이었음에도 그렇게 하지 못한 것이 안타깝게 느껴집니다. 개인적으로는 박사 과정 수학을 하면서 연구에 대한 좀 더 깊은 이해와 지식을 다질 수 있었으며, 연구뿐만이 아니라 삶에 있어서도 어떠한 것이 더 중요한 것인지를 치열하게 생각해 볼 수 있었던 시간이었습니다.

먼 곳에 있었지만 항상 마음으로 후원해 주시고 사랑을 아끼지 않으셨던 아버지, 어머니, 그리고 동생에게도 감사드립니다. 좋을 때나 나쁠 때나 항상 같은 곳을 바라보며 마음에 힘이 되었던 윤정이와 윤정이의 가족들에게도 감사드립니다. 그리고 무엇보다도 가장 큰 마음의 힘이 되었으며, 학위 논문을 작성할 수 있도록 연구의 지혜를 주시고, 건강하게 학위 과정을 마칠 수 있도록 하루 하루를 베풀어 주신 하나님께 감사드립니다.

Curriculum Vitae

Name : Cho, Jeong-woo
Date of Birth : September 17, 1978
Birthplace : Geoje Island, Republic of Korea
Domicile : Geoje Island, Republic of Korea
E-mail : ggumdol@netsys.kaist.ac.kr

Educations

1994. 3. – 1996. 2. Gyeongnam Science High School
1996. 3. – 2000. 2. Dept. of Electrical Engineering and Computer Science
(Division of Electrical Engineering), KAIST (B.S.)
2000. 3. – 2002. 2. Dept. of Electrical Engineering and Computer Science
(Division of Electrical Engineering), KAIST (M.S.)
2002. 3. – 2005. 8. Dept. of Electrical Engineering and Computer Science
(Division of Electrical Engineering), KAIST (Ph.D.)

International Journal Papers

- [J1] **Jeong-woo Cho** and Dong-ho Cho, "Dynamic Buffer Management Scheme Based on Rate Estimation in Packet-Switched Networks", *Computer Networks*, vol. 39, no. 6, pp. 769-787, August 2002.
- [J2] Hyung-Keun Ryu, **Jeong-woo Cho** and Song Chong, "Stabilized Edge-to-Edge Aggregate Flow Control", *Lecture Notes in Computer Science*, vol. 3042, pp. 574-587, 2004.
- [J3] **Jeong-woo Cho** and Song Chong, "Stabilized Max-Min Flow Control Using PID and PII² Controllers", to appear in the *IEICE Trans. Communications*.
- [J4] Hyang-Won Lee, **Jeong-woo Cho** and Song Chong, "A Distributed Max-Min Flow Control Algorithm for Multi-rate Multicast Flows", submitted to the *IEEE Trans. Communications*.
- [J5] **Jeong-woo Cho** and Song Chong, "Utility Max-Min Flow Control Using Slope-Restricted Utility Functions", submitted to the *IEEE Trans. Communications*.
- [J6] **Jeong-woo Cho**, Seong-Lyun Kim and Song Chong, "Infrastructure Support Increases the Capacity of Ad Hoc Wireless Networks", submitted to the *IEEE Communications Letters*.

International Conference Papers

- [C1] **Jeong-woo Cho** and Dong-ho Cho, "A Dynamic Buffer Management Scheme Based on Rate Estimation in Packet-Switched Networks", in *Proceedings of IEEE Globecom 2001*, San Antonio, Texas, November 2001, pp. 2304–2310.
- [C2] **Jeong-woo Cho**, Taesoo Kwon, Changhoi Koo, DS Park, Daegyun Kim and Dong-ho Cho, "Multiple Quality Control: A New Framework for QoS Control in Forward Link of 1xEV-DV Systems", in *Proceedings of IEEE VTC 2002 Spring*, Birmingham, Alabama, May 2002, vol. 3, pp. 1165–1169.

- [C3] Hyung-Keun Ryu, **Jeong-woo Cho** and Song Chong, "Stabilized Edge-to-Edge Aggregate Flow Control", in *Proceedings of IFIP Networking 2004*, Athens, Greece, May 2004, pp. 574–587.
- [C4] **Jeong-woo Cho** and Song Chong, "Stabilized Max-Min Flow Control Using PID and PII² Controllers", in *Proceedings of IEEE Globecom 2004*, Dallas, Texas, November 2004, pp. 1411–1417.
- [C5] Hyang-Won Lee, **Jeong-woo Cho** and Song Chong, "A Distributed Max-Min Flow Control Algorithm for Multi-rate Multicast Flows", in *Proceedings of IEEE Globecom 2004*, Dallas, Texas, November 2004, pp. 1140–1146.
- [C6] **Jeong-woo Cho**, Seong-Lyun Kim and Song Chong, "Infrastructure Support Increases the Capacity of Ad Hoc Wireless Networks", in *Proceedings of IEEE VTC 2005 Fall*, Dallas, Texas, September 2005.
- [C7] **Jeong-woo Cho** and Song Chong, "Utility Max-Min Flow Control Using Slope-Restricted Utility Functions", in *Proceedings of IEEE Globecom 2005*, Saint Louis, Missouri, November 2005.

Patents

- [P1] 배범식, 조동호, 정영욱, 조정우, 권태수, 정정수, 구창희, "이동통신 시스템에서 역방향 데이터 전송 제어 방법," Korea, November 2001.
- [P2] Beom-Sik Bae, Dong-Ho Cho, Young-Wook Jung, **Jeong-woo Cho**, Tae-Soo Kwon, Jung-Su Jung and Chang-Hoi Koo, "Method of controlling reverse data transmission in a mobile communication system," USA, November 2003.

Grants

- [G1] 2004, Student Travel Grant for IEEE Globecom 2004, IEEE Communications Society.